The Stereological and Statistical Properties of Entrained Air Voids in Concrete: A Mathematical Basis for Air Void System Characterization

by

Kenneth Snyder
Building and Fire Research Laboratory
National Institute of Standards and Technology
Gaithersburg, MD 20899 USA

and

Kumar Natesaiyer
USG Research Center
Libertyville, IL USA

and

Kenneth Hover
Cornell University
Ithaca, New York 14853 USA

Reprinted from Materials Science of Concrete VI, Sidney Mindess and Jan Skalny, eds., The American Ceramic Society, 735 Ceramic Place, Westerville, OH 43081, pp. 129-214, 2001.

NIST
National Institute of Standards and Technology
Technology Administration, U.S. Department of Commerce

The Stereological and Statistical Properties of Entrained Air Voids in Concrete: A Mathematical Basis for Air Void System Characterization

Kenneth Snyder
National Institute of Standards and Technology, Gaithersburg, Maryland

Kumar Natesaiyer
USG Research Center, Libertyville, Illinois

Kenneth Hover
Cornell University, Ithaca, New York

> *"Yet I exist in the hope that these memoirs, in some manner, I know not how, may find their way to the minds of humanity in Some Dimension, an may stir up a rave of rebels who shall refuse to be confined to limited Dimensionality."*
>
> — Edwin Albott

To understand the freeze-thaw properties of hardened concrete, the air void system microstructure must be characterized. Studies of the stereological and statistical properties of entrained air voids in concrete have often involved a number of steps: sample preparation and air void identification, linear and planar analysis of a polished surface, uncertainty analysis of the recorded data, parametric and nonparametric estimates of the air void diameter distribution, and analysis of the air void system spatial statistics. Each of these steps has been discussed in detail in a number of engineering fields. For the civil engineering researcher, a comprehensive study of these properties requires consulting many varied texts, each addressing these steps individually. This chapter attempts to consolidate these topics, critically review them, and combine them into a single desk reference. The researcher can then realize the interdependencies of these topics, learn to accurately characterize the air void system microstructure, and develop an understanding of the basis for standardized test methods such as ASTM C 457.

Introduction

The effectiveness of air entrainment in providing frost resistance to concrete is well known to the industry. Though there are differing hypotheses on the mechanism of frost damage, all the mechanisms suggest that frost

durability is a function of the material properties of the concrete, the freezing environment to which it is subjected, and the air void system in the concrete. Despite this knowledge, the frost resistance of concrete is commonly evaluated using air void parameters alone. The common air void parameters used are air content by volume, the specific surface area, and the Powers spacing factor. These values are calculated for hardened concrete using the standard test method ASTM C 457.[1]

When actual freeze/thaw testing is not feasible, it is common to predict the frost resistance of concrete on the basis of air void geometry alone. To make such a prediction, a small fraction of the air voids present in the hardened concrete are observed through a microscope, and statistical inferences are drawn about the population of the air voids as a whole.[2]

Given that a cubic meter of concrete may contain on the order of 10^{10} air voids, and that a conscientious microscopic evaluation might sample 10^3 voids, it is clear that the issues of statistical inference and uncertainty are central to geometric analysis. Accurately assessing the air void system is further complicated by the fact that information is needed about the three-dimensional air void characteristics, but observations are made on the two-dimensional intersection of the void with the plane. In a typical analysis performed in accordance with ASTM C 457, no attempt is made to measure the diameter of an actual air void, nor is any attempt made to measure the diameter of the intersection between the void and the two-dimensional plane. Even this most basic of geometric characteristics of a single void is inferred from a large number of observations, none which are intentionally of the actual air void diameter.

The descriptive geometry of the three-dimensional air void system is complicated still further by the need to know something about the spatial distribution of the voids. Once again, in a standard ASTM C 457 analysis, no data are collected about the actual location or spatial distribution of the voids. All of this is later inferred on the basis of a priori assumptions or structural models, irrespective of the actual concrete microstructure. The industry's ability to correlate actual frost resistance with air void system geometry attests to the fact that the mathematical approaches developed over the years have been able to deal with these complications to varying degrees.

There is considerable room for improvement of the current state of practice, however. First, there is not a broad understanding of the fundamental uncertainty that accompanies air void interpretation. The apparent complexity of the equations used in standard practice too often causes the practi-

tioner to assume more accuracy and precision than can be justified. Second, the availability of computers means that we need not confine ourselves to oversimplified geometric models for reasons of computational expediency. More useful techniques are available than those currently used in practice. Perhaps this chapter will serve to clarify the mathematical background of the problem, emphasize the uncertainty inherent in various approaches, and suggest improved techniques.

Background

Since the 1940s, it has been known that the addition of a small volume of entrained air voids into concrete has a dramatic effect upon performance under freezing and thawing conditions. Since then, numerous reports have been published that discuss ways to characterize the air void system in concrete. One of the first attempts, and perhaps the most famous in the concrete research community, was the spacing equation proposed by Powers in 1949.[3] The equation that bears his name exists today as part of ASTM C 457, which is the standard test method for characterizing air voids in hardened concrete.

The Rosiwal technique[4] that is the basis for ASTM C 457 dates back to 1898. Brown and Pierson[5] were among the first researchers to apply this technique to the study of air voids. Today, the test is used to estimate the volume fraction of entrained air, the surface area of air voids per volume of air voids (specific surface area), and the Powers spacing factor. However, this is as far as the standardized test goes with respect to characterizing the air void system in concrete.

The methods for characterizing the uncertainty in measured volumetric quantities obtained from the ASTM C 457 method have been published in various sources. The techniques are rather straightforward, but have not been delineated for all three methods of ASTM C 457. Although there is an ASTM standard practice for calculating uncertainty (ASTM D 4356), this practice has not yet been incorporated into ASTM C 457. This is unfortunate, since the calculations for the point count, linear traverse, and modified point count methods have been published and are available. The individual results have been combined here for completeness.

More sophisticated techniques for characterizing spheres embedded within a matrix have been developed by concrete materials researchers and metallurgists, among others. Wicksell[6] was one of the first researchers to address the problem of reconstructing properties of the particle size distribution based upon data collected on a thin section. Others, such as Reid,[7] advanced

these ideas to plane section analysis. Subsequent publications completed the remaining mathematical components required to allow one to easily transform among data collected in one-, two-, and three-dimensions.

The issue of "air void spacing" equations has been addressed a number of times since the 1949 equation by Powers.[3] Notably, Philleo,[8] Fagerlund,[9] Pleau and Pigeon,[10] and Attiogbe[11] have each contributed equations. Each equation addresses the topic differently. Also, the lack of consistent terminology has obfuscated discussions of the equations. The equations are discussed here with summary descriptions of each spacing equation. Results from previous numerical[12] and analytical[13] tests of the equations are also discussed.

Purpose

This chapter consolidates most of the information regarding the characterization of air voids in concrete. It is both interesting and unfortunate that the information contained in this chapter has not been summarized previously. The book by Underwood[14] is comprehensive, but it does not contain uncertainty equations sufficient for ASTM C 457, the inversion formulae in analytical form, sophisticated spacing equations, or the concept of protected paste volume. The hope is that this chapter will both serve as a clearinghouse for this information and also express all of this information within a single context. True understanding begins when one is able to look beyond a piece of information and see how this piece interrelates with the whole.

Once compiled, the information contained in this chapter should be of great value to anyone modeling the air void microstructure within concrete. To successfully model the air void system, one must be able to accurately characterize both the size distribution and the proximity of the voids to either one another or to points within the paste. This chapter discusses this in detail for both plane section and thin section analyses.

Finally, although this chapter serves as a useful starting point for future concrete research, it has also been developed with the intent of highlighting what information is still needed. To this end, each section within this chapter includes a discussion of existing research needs.

Quantitative Stereology

Quantitative stereology is the body of methods for quantifying properties of a three-dimensional composite using only the data present on either a plane surface or thin section that intersects that composite. Typically, the objects of interest are discrete entities within a host matrix. Historically, many of

the advances in quantitative tools have been developed for solving problems in biology and metallurgy. The field traces most of the theoretical ground work back to Wicksell,[6] who was seeking to quantify the geometrical character of cells on a microscopic thin section of tissue. More recently, metallurgists have been making advances in quantifying irregularly shaped objects, as one might find in certain alloys.

The most useful single reference on this subject is the book *Quantitative Stereology* by Underwood.[14] The book covers much of the theoretical work on quantifying volumetric data. It is an excellent source for proofs of why linear and planar probes are unbiased estimators of volumetric quantities such as volume fraction.

Plane Section

In order to perform a quantitative analysis, a system is often penetrated by a plane section. The intersection of the plane with the spherical air voids creates circles. Since concrete is an opaque material, it may be difficult to visualize the connection between the circles and the spherical voids. Figure 1 shows a three-dimensional void system intersecting a plane. The intersection of the voids with the plane is depicted by a black circle; most of the spheres are below the plane and so do not intersect it. As one can readily see, the size of the intersected circle may not be representative of the intersected sphere radius. However, when considered on the whole, the distribution of circle diameters can yield useful information about the distribution of sphere radii.

The air void microstructure depicted in Fig. 1 shows a system of nonoverlapping spheres. It will be assumed throughout this chapter that the air void system is composed of distinct spherical voids. This a priori assertion will receive further discussion in subsequent sections.

Probes

When performing a stereological analysis, the experimenter chooses the type of probe to use. Possible probes include points, lines, surfaces, or volumes. Concrete petrographers are typically most familiar with point probes (point count) and linear probes (linear traverse). ASTM C 457, based upon the work of Brown and Pierson,[5] includes both methods, and a third method (modified point count) that is a combination of the two. The use of a planar probe to analyze air voids in concrete has been discussed by Verbeck.[15] However, the standardized method has adopted the point and linear probe analyses due to their simplicity.

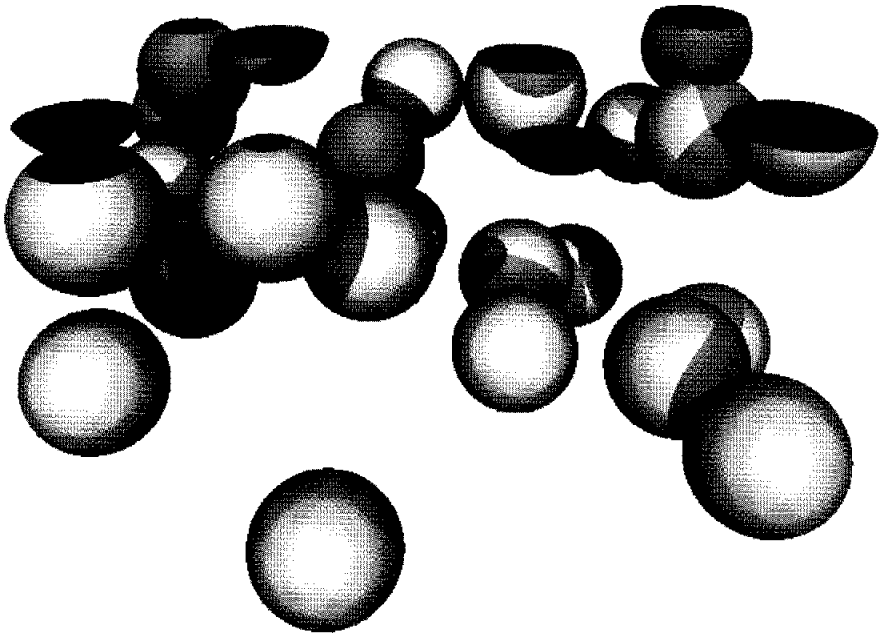

Figure 1. Three-dimensional view of a random plane intersecting a system of monosized spheres. The intersection of the plane with a sphere is denoted by a black circle.

The choice of a probe depends upon the quantity desired. Point probes are sufficient for determining the volume fractions. To characterize geometrical quantities, probes of higher dimensionality are required. Linear probes are sufficient for characterizing the size and spacing of the air voids. Estimates of the number of voids in a given volume of concrete can be calculated from planar probe data, but only approximated from linear probe data.

Since the point and linear probes are used in ASTM C 457, they are discussed in detail here. A schematic of a point probe is shown in Fig. 2(a), and a linear probe analysis is shown in Fig. 2(b). The figure represents the intersection of a plane with a matrix containing spheres of a constant radius. Since the location of each sphere is random (but not overlapping another sphere), the circles of intersection between the spheres and the plane do not all have the same radius. The image in Fig. 2(a) contains small filled circles that delineate the locations of the point probe analysis. Similarly, the image in Fig. 2(b) contains horizontal lines that delineate the path of a linear probe over the surface. One could also imagine performing a planar probe analysis by simply recording the radius of each circle intersecting the plane.

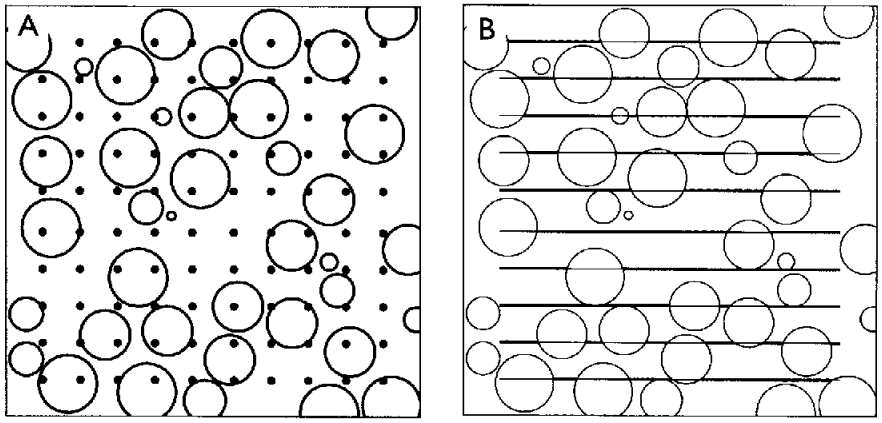

Figure 2. Schematic of a plane surface through a matrix containing mono-sized spheres. The points in (a) delineate a point probe analysis; the horizontal lines in (b) delineate a linear probe analysis.

Volumetric Statistical Properties

The methods of stereology are often used to characterize particles. The particles could either be separate entities or be part of a composite. The composite could be composed of either discrete particles in a matrix or space-filling particles like alloys in a metal. For the case of air voids in concrete, the following discussion will concentrate on discrete particles embedded in a matrix.

The methods discussed here are not used to characterize an individual particle. Since a composite may consist of millions of particles, this approach would be meaningless. Rather, a more useful goal is to characterize the collection of particles that are of interest by estimating useful statistical properties such as the volume fraction and the surface area.

Volume Fraction

One of the most informative statistical properties is the volume fraction of a particular phase of interest. According to Underwood,[14] the idea was outlined by Delesse,[16] and a number of mathematical derivations exist by Hilliard,[17] Chayes,[18] and Saltykov.[19] The following mathematical description follows those of Weibel[20] and McLean.[21] For some phase α within a composite of total volume V_T, the volume of the α-phase is V_α. The ratio of the volumes is the volume fraction ϕ_α of phase α:

$$\phi_\alpha = \frac{V_\alpha}{V_T} \tag{1}$$

Let the composite be a cube with edge length L. The cube is oriented along a Cartesian coordinate system, and a cut is made perpendicular to the z-axis. On the surface of the cut are intersections with the inclusions of phase α. Let the indicator function a_α represent the location of the α-phase on the plane:

$$a_\alpha = \begin{cases} 1 & \alpha \text{ phase at } (x, y, z) \\ 0 & \text{otherwise} \end{cases} \tag{2}$$

The surface area A_α of the α-phase on the plane located at z is the integral of a_α over the area A_T of the plane section:

$$A_\alpha = \int_{A_T} a_\alpha(x, y \mid z)\, dx\, dy \tag{3}$$

Replace the cut by a slice with differential thickness dz. The total volume of the α-phase is the integral of A_α:

$$V_\alpha = \int A_\alpha(z)\, dz \tag{4}$$

Let the total planar surface area be $A_T = L^2$. The ratio of volumes can be expressed as a function of $A_\alpha(z)$:

$$\frac{V_\alpha}{V_T} = \frac{\int A_\alpha(z)\, dz}{L A_T} \tag{5}$$

The integral is an average:

$$\frac{V_\alpha}{V_T} = \frac{\overline{A_\alpha}}{A_T} \tag{6}$$

Therefore, an estimate of the area fraction of the phase α is an unbiased estimator of the volume fraction of the phase α, in as much as $A_\alpha(z)$ is an unbiased estimator of $\overline{A_\alpha}$.

This approach can be extended to both linear and point probes. Consider the plane section A_T discussed above. Pass a line, perpendicular to the y-axis, across the surface. Let the indicator function l_α represent the location of the α-phase along the line:

$$l_\alpha = \begin{cases} 1 & \alpha \text{ phase at } (x,y,z) \\ 0 & \text{otherwise} \end{cases} \tag{7}$$

The total length $L_\alpha$of the α-phase along the line is the integral of l_α:

$$L_\alpha(y,z) = \int l_\alpha(x \mid y,z)\, dx \tag{8}$$

Replace the line with a ribbon with differential width dy. The total area of the α-phase on the surface is the integral of L_α:

$$A_\alpha(z) = \int L_\alpha(y,z)\, dy \tag{9}$$

The ratio of areas can be expressed as a function of $L_\alpha(y,z)$:

$$\frac{A_\alpha(z)}{A_T} = \frac{\int L_\alpha(y,z)\, dy}{L^2} \tag{10}$$

As in the case of the area average, this integral can also be expressed as an average:

$$\frac{A_\alpha(z)}{A_T} = \frac{\overline{L_\alpha(z)}}{L} \tag{11}$$

Therefore, the lineal fraction of phase α along a lineal probe is equal to the area fraction of that phase, which is in turn equal to the volume fraction. The mathematical framework for point probes proceeds in the same manner by constructing lines from points.

This entire development was performed without addressing randomness in either the α-phase or the locations of the probes. This issue arises when asserting that $A_\alpha(z) = \overline{A_\alpha}$. This statement assumes that the area fraction exposed at some value of z is representative of any other $A_\alpha(z)$. This kind of assumption is also made for the linear and point probes. The final result is

that the linear fraction of phase α of a linear probe is an unbiased estimation of the volume fraction of phase α. Likewise, the number fraction of points landing on phase α is an unbiased estimation of the volume fraction of phase α.

Surface Area

Another useful characteristic of particles within a matrix is the particle surface area. Within a volume V_T there are particles with total surface area S_α and total volume V_α. The average surface area per particle is S_α/V_α. A linear probe analysis of total length L_T is composed of N_α chords over the α-phase. The total length of chords over the α-phase is L_α, and the average chord length is $\overline{L_\alpha} = L_\alpha/N_\alpha$. The total surface area of particles can be calculated using the equation of Saltykov[22]:

$$\frac{S_\alpha}{V_T} = \frac{4N_\alpha}{L_T} \tag{12}$$

This quantity is sometimes referred to as the specific surface. However, in the concrete research literature the quantity of interest has been $\overline{S_\alpha} / \overline{V_\alpha}$, and has been derived by Tomkeieff[23] and Chalkley et al.[24]:

$$\frac{\overline{S_\alpha}}{\overline{V_\alpha}} = \frac{4N_\alpha}{L_\alpha} = \frac{4}{\bar{l}} \tag{13}$$

The quantity $\bar{l}$ is the average chord length, as defined by ASTM C 457. This quantity is also referred to as the specific surface, and will be the default definition for subsequent discussions of air void specific surface.

ASTM C 457 Uncertainty Analysis

Interest in the expressed uncertainty in the results of a linear traverse analysis of air voids dates back to the paper of Verbeck.[15] Not long after, Brown and Pierson,[5] Willis,[25] and Mather[26] used uncertainty arguments for improving the test method. An interlaboratory comparison by Sommer[27] was one of the first attempts to relate theoretical and practical uncertainties.

While the uncertainty in point and linear analyses of volumetric data have been known for some time,[14] contribututions have been made to the specific tasks associated with ASTM C 457. Expressions for the uncertainty for the modified point count method have been given by Langan and Ward[28]

and Pleau and Pigeon.[29] Expressions for the linear traverse method have been given by Snyder et al.[30] These results are presented here as a summary.

Details of the uncertainty calculations are given in Appendix A. In summary, let the calculated quantity y be a function of N different measured quantities x_n. The dispersion in each x_n value represents the standard uncertainty $u(x_n)$ in the estimate of x_n. The combined standard uncertainty $u_c(y)$ in y is a function of the individual uncertainties $u(x_n)$:

$$u_c^2(y) = \sum_{n=1}^{N} \left(\frac{\partial y}{\partial x_n} \right)^2 u^2(x_n) + 2 \sum_{m=1}^{N-1} \sum_{n=m+1}^{N} \frac{\partial y}{\partial x_m} \frac{\partial y}{\partial x_n} u(x_m, x_n) \tag{14}$$

To say something quantitative about the calculated value y, one must define a coverage factor k that is used to produce an expanded uncertainty $U_p = ku_c(y)$ that defines an interval $Y = y \pm U_p$ having an approximate level of confidence p. For a Gaussian error model, a coverage factor k equal to 2 will have nearly a 95 % level of confidence. This is the familiar "two-sigma" interval.

For brevity, the notation $u_c^2(y)$ will be shortened to s_y^2 and will serve as an estimated standard deviation. It will be assumed that when the subscript to s^2 is a calculated quantity, the uncertainty in question is a combined standard uncertainty. The coefficient of variation will be represented by the variable C.

It should be noted that these calculations characterize an idealization. The equations reflect the minimum uncertainty that a perfect operator, using equipment with infinite resolution, can state from the result of one planar analysis of a perfectly prepared specimen. Errors due to improper identification of voids, improper sample preparation, and insufficient magnification add to these minimum uncertainties. While each of these factors is an important component to the overall uncertainty, it is critical to at least be able to quantify the uncertainty in the ideal case. Once these have been outlined, one can then begin to quantify the impact of the other sources of error.

Random Processes

The measurement methods of ASTM C 457 include both point count and linear traverse. Although the results from both techniques are random, the statistics differ. The difference is small, but important.

The outcome from a point count experiment is characterized by the bino-

mial distribution. Assume that an operator seeks to characterize the air content within a piece of concrete. The operator will perform a point count consisting of S_t total stops. The probability that an individual point lands over air is q. The probability of not landing over air is $1-q$. The outcome from an experiment is S_a points over air. The estimated variance in the number of points over air is calculated from the binomial distribution:

$$\begin{aligned} s_{S_a}^2 &= S_t\, q\,(1-q) \\ &= S_t \frac{S_a}{S_t}\left(1-\frac{S_a}{S_t}\right) \end{aligned} \tag{15}$$

The square of the coefficient of variation is a simple result:

$$\begin{aligned} C_{S_a}^2 &= \left(\frac{s_{S_a}}{S_a}\right)^2 \\ &= \frac{1}{S_a}-\frac{1}{S_t} \end{aligned} \tag{16}$$

The modified point count and the linear traverse require a similar quantity. During the test, the number of chords intersected N_a is recorded. The intersection of randomly placed air voids is a Poisson process.[31] Therefore, the variance in the number of chords recorded is equal to the number of chords:

$$s_{N_a}^2 = N_a \tag{17}$$

The coefficient of variation is similar to the point count value above:

$$C_{N_a}^2 = \frac{1}{N_a} \tag{18}$$

The difference between the result for C_{S_a} and for C_{N_a} is due to the difference between continuum and discrete sampling; this distinction seems to be missing in the mathematical development of Langan and Ward.[28] Note that as S_t approaches infinity, the value of $C_{S_a}^2$ approaches $1/S_a$, which is analogous to the result for N_a.

Point Count

The point count technique is probably the oldest, and best characterized, tool for petrographic characterization. Because it is a point probe, it is limited as to the volumetric information it can yield. Specifically, the point count method estimates the volume fraction of a particular phase of interest.

While performing an ASTM C 457 point count analysis, the operator records information regarding both the air and the paste:

S_a: number of stops over air

S_p: number of stops over paste

S_t: total number of stops

The desired quantities are the volume fraction of air A and paste p:

$$A = \frac{S_a}{S_t} \qquad p = \frac{S_p}{S_t} \tag{19}$$

Since the total number of stops S_t is fixed, the uncertainty in each volume fraction is proportional to the uncertainty in the number of stops over the phase of interest:

$$C_A^2 = C_{S_a}^2 = \frac{1}{S_a} - \frac{1}{S_t} \qquad C_p^2 = C_{S_p}^2 = \frac{1}{S_p} - \frac{1}{S_t} \tag{20}$$

Linear Traverse

The ASTM C 457 linear traverse technique is a linear probe analysis of concrete containing air entrainment. The operator records the "chords" where the line intersects the phase of interest. As currently written, the operator is required only to record the length of linear probe over the spherical air voids and the cumulative length of the chords. However, the analysis that follows assumes that the operator also records the lengths of the individual chords. This should not be an arduous task since modern laboratory equipment designed for this test is computerized. The uncertainty analysis that follows has been addressed previously.[28,30]

Upon completion of the linear traverse, the reported quantities are as follows:

N_a: number of air chords

T_t: length of entire traverse

T_a: length of traverse over air

$\bar{l}$: average chord length

For the purpose of this analysis, the uncertainty in the total traverse length T_t is assumed to be zero. The uncertainty in the reported quantities will depend upon the uncertainty in the measured quantities:

$$s_{N_a}^2 = N_a \qquad s_{\bar{l}}^2 = \frac{s_l^2}{N_a} \tag{21}$$

Air Content

The analysis of the uncertainty in the air volume fraction begins by expressing the air content A in terms of measured quantities:

$$A = \frac{N_a \bar{l}}{T_t} \tag{22}$$

The coefficient of variation in A is a function of these variables:

$$\left(\frac{s_A}{A}\right)^2 = \left(\frac{T_t}{N_a \bar{l}}\right)^2 \left[\left(\frac{\partial A}{\partial N_a}\right)^2 s_{N_a}^2 + \left(\frac{\partial A}{\partial \bar{l}}\right)^2 s_{\bar{l}}^2\right]$$

$$C_A^2 = \frac{1}{N_a}\left[1 + C_l^2\right] \tag{23}$$

This result has been reported elsewhere.[30,31]

Specific Surface

The specific surface is calculated from the average chord length $\bar{l}$:

$$\alpha = \frac{4}{\bar{l}} \tag{24}$$

Assuming a Gaussian error model for $\bar{l}$, the variance in α is infinite[32] because of the nonzero probability of a negative $\bar{l}$. Nonetheless, one proceeds under the assumption that the normal distribution that characterizes $\bar{l}$ is localized: $C_{\bar{l}} << 1$ This is reasonable since N_a is typically on the order of 1000.

On the basis of this assumption, the coefficient of variation in α can be calculated from the measured quantity $\bar{l}$:

$$\left(\frac{s_\alpha}{\alpha}\right)^2 = \left(\frac{\bar{l}}{4}\right)^2 \left(\frac{\partial \alpha}{\partial \bar{l}}\right)^2 s_{\bar{l}}^2$$

$$C_\alpha^2 = \frac{1}{N_a} C_l^2 \tag{25}$$

Spacing Factor

The analysis for the Powers spacing factor is divided into separate parts for the two equations that apply. When the ratio p/A is less than 4.342, for reasons to be discussed in a subsequent section, the spacing factor $\bar{L}$ has the following relationship:

$$\bar{L} = \frac{p\,T_t}{4\,N_a} \tag{26}$$

The coefficient of variation in $\bar{L}$ is

$$\left(\frac{s_{\bar{L}}}{\bar{L}}\right)^2 = \left(\frac{4\,N_a}{p\,T_t}\right)^2 \left[\left(\frac{\partial \bar{L}}{\partial p}\right)^2 s_p^2 + \left(\frac{\partial \bar{L}}{\partial N_a}\right)^2 s_{N_a}^2\right]$$

$$C_{\bar{L}}^2 = C_p^2 + \frac{1}{N_a} \tag{27}$$

When the ratio p/A is greater than 4.342, as it should be for most concretes containing entrained air,[3] the spacing factor has the following form:

$$\bar{L} = \frac{3}{\alpha}\left[1.4\left(1 + \frac{p}{A}\right)^{1/3} - 1\right]$$

$$= \frac{3\,\bar{l}}{4}\left[1.4\left(1 + \frac{p\,T_t}{N_a\,\bar{l}}\right)^{1/3} - 1\right] \tag{28}$$

The coefficient of variation can be expressed as

$$\left(\frac{s_{\bar{L}}}{\bar{L}}\right)^2 = \frac{1}{\bar{L}^2}\left[\left(\frac{\partial \bar{L}}{\partial \bar{l}}\right)^2 s_{\bar{l}}^2 + \left(\frac{\partial \bar{L}}{\partial p}\right)^2 s_p^2 + \left(\frac{\partial \bar{L}}{\partial N_a}\right)^2 s_{N_a}^2\right]$$

$$C_{\bar{L}}^2 = \frac{(1-\beta)^2}{N_a} C_{\bar{l}}^2 + \beta^2\left(C_p^2 + \frac{1}{N_a}\right) \tag{29}$$

Here, the result has been made more compact through an intermediate quantity β:

$$\beta = \frac{\bar{l}}{\bar{L}}\left(\frac{1.4}{4}\right)\left(\frac{p}{A}\right)\left(1+\frac{p}{A}\right)^{-2/3} \tag{30}$$

These results represent the general approach of Snyder et al.,[30] Langan and Ward,[28] and Warris.[33] The final result of Langan and Ward is identical, but the answer was simplified by eliminating terms that have a negligible contribution[28]:

$$C_{\bar{L}}^2 = \beta^2\left[C_p^2 + C_A^2\right] \tag{31}$$

Modified Point Count

The modified point count method is a mixture of the point count and the linear traverse methods. The operator performs a point count on each line, then reanalyzes the line to record the number of air voids intersected. The uncertainty in this method has been addressed by Pleau and Pigeon.[29] The measured quantities are as follows:

N_a: number of air chords
S_t: total number of stops
S_a: number of stops over air
I: distance between stops

Air Content

The air content is simply the ratio of stops over air to the total number of stops, as in the point count method:

$$A = \frac{S_a}{S_t} \tag{32}$$

As discussed before, the coefficient of variation in the air content A follows from the binomial distribution:

$$C_A^2 = \frac{1}{S_a} - \frac{1}{S_t} \tag{33}$$

Specific Surface

The specific surface equation depends upon both point probe and lineal probe data:

$$\alpha = \frac{4\,N_a}{S_a\,I} \tag{34}$$

The coefficient of variation in α is calculated in the same manner as before:

$$\left(\frac{s_\alpha}{\alpha}\right)^2 = \left(\frac{N_a}{4\,S_a\,I}\right)^2 \left[\left(\frac{\partial\,\alpha}{\partial\,S_a}\right)^2 s_{S_a}^2 + \left(\frac{\partial\,\alpha}{\partial\,N_a}\right)^2 s_{N_a}^2\right]$$

$$C_\alpha^2 = \frac{1}{S_a} - \frac{1}{S_t} + \frac{1}{N_a} \tag{35}$$

Spacing Factor

When the ratio p/A is less than 4.342, the Powers spacing factor $\overline{L}$ has the following relationship:

$$\overline{L} = \frac{p}{\alpha\,A} = I\,\frac{p\,S_t}{4\,N_a} \tag{36}$$

The coefficient of variation will depend only upon the uncertainty in the paste content and the number of chords:

$$\left(\frac{s_{\overline{L}}}{\overline{L}}\right)^2 = C_p^2 + \frac{1}{N_a} \tag{37}$$

When the ratio p/A is greater than 4.342, the spacing factor $\bar{L}$ has the following relationship:

$$\bar{L} = \frac{3\,S_a\,I}{4\,N_a}\left[1.4\left(1+\frac{S_p}{S_a}\right)^{1/3} - 1\right] \tag{38}$$

The equation for the coefficient of variation resembles that for the linear traverse method:

$$\left(\frac{s_{\bar{L}}}{\bar{L}}\right)^2 = \left(\frac{\partial\,\bar{L}}{\partial\,N_a}\right)^2 s_{N_a}^2 + \left(\frac{\partial\,\bar{L}}{\partial\,S_a}\right)^2 s_{S_a}^2 + \left(\frac{\partial\,\bar{L}}{\partial\,p}\right)^2 s_p^2$$
$$C_{\bar{L}}^2 = C_{N_a}^2 + \beta^2\,C_p^2 + (1-\beta)^2\,C_{S_a}^2 \tag{39}$$

The value of β is the same as for the linear traverse case:

$$\beta = \frac{I\,S_a}{\bar{L}\,N_a}\left(\frac{1.4}{4}\right)\left(\frac{p\,S_t}{S_a}\right)\left(1+\frac{p\,S_t}{S_a}\right)^{-2/3} \tag{40}$$

This result for the Powers spacing factor coefficient of variation differs slightly from that of Pleau and Pigeon.[29]

Paste Content

In the preceding discussion, the relative uncertainty in the paste content C_p of the concrete has been left undefined. Currently, ASTM C 457 does not specify how the paste content shall be determined for either the linear traverse or the modified point count methods. Therefore, experimenters have been left to their own discretion. Two methods present themselves: record stops over paste during the modified point count method, or record individual paste chords during a linear traverse. By evaluating the paste volume fraction like the air volume fraction, the preceding sections that address uncertainty in air content A can be used to likewise determine uncertainty in the paste content p.

Example

The following example of an uncertainty calculation for ASTM C 457 is based upon data given in Ref. 30 that included results for individual paste

chords. The average and standard deviation of the paste chords are represented by $\overline{\pi}$ and σ_π, respectively. The uncertainties reported below represent an estimate of two standard deviations. This corresponds to an approximate coverage factor of 95%.

The data in Ref. 30 are for a linear traverse that included measurements of individual paste chords. The data that appear below for the point count and modified point count are based upon these data. Also, the data are consistent among the methods.

Point Count

The following data are fictitious, but are based upon the data given in Ref. 30:

$$S_t = 1000 \qquad S_a = 57 \qquad S_p = 311$$

The coefficient of variation for the air content A and paste content p can be calculated directly:

$$C_A^2 = \frac{1}{S_a} - \frac{1}{S_t} = 0.0165 \qquad C_p^2 = \frac{1}{S_p} - \frac{1}{S_t} = 0.0022$$

The reported volume fractions are also calculated directly:

$$A = \frac{S_a}{S_t}\left[1 \pm 2\, C_A\right] = (5.7 \pm 1.4)\,\%$$

$$p = \frac{S_p}{S_t}\left[1 \pm 2\, C_p\right] = (31.1 \pm 2.9)\,\%$$

Linear Traverse

The following linear traverse data can be found in Ref. 30: $N_a = 1420$, $N_p = 3447$, $\overline{l} = 0.1126$ mm, $\overline{\pi} = 0.2569$ mm, $\sigma_l = 0.2536$ mm, and $\sigma_\pi = 0.8048$ mm. The total length of the traverse is L_T is 2656 mm.

The coefficient of variation for the volume fractions are as follows:

$$C_A^2 = \frac{1}{N_a}\left[1 + C_l^2\right] = 0.00428 \qquad C_p^2 = \frac{1}{N_p}\left[1 + C_\pi^2\right] = 0.00314$$

The reported volume fractions, to two standard deviations, are as follows:

$$A = \frac{N_a \bar{l}}{L_T}\left[1 \pm 2\, C_A\right] = (6.02 \pm 0.79)\,\%$$

$$p = \frac{N_p \bar{\pi}}{L_T}\left[1 \pm 2\, C_p\right] = (33.4 \pm 3.7)\,\%$$

The coefficient of variation for the specific surface is as follows:

$$C_\alpha^2 = \frac{1}{N_a} C_l^2 = 0.00357$$

The specific surface, reported to two standard deviations, is calculated from

$$\alpha = \frac{4}{\bar{l}}\left[1 \pm 2\, C_\alpha\right] = (35.5 \pm 4.2)\ \text{mm}^{-1}$$

The calculation for the Powers spacing factor $\bar{L}$ is a little more involved. First, the spacing factor is calculated:

$$\bar{L} = \frac{3\bar{l}}{4}\left[1.4\left(1 + \frac{N_p \bar{\pi}}{N_a \bar{l}}\right)^{1/3} - 1\right] = 0.1366\ \text{mm}$$

This is used to calculate β:

$$\beta = \frac{\bar{l}}{\bar{L}}\left(\frac{1.4}{4}\right)\left(\frac{p}{A}\right)\left(1 + \frac{p}{A}\right)^{-2/3} = 0.4574$$

The quantity β is then used to calculate the coefficient of variation in $\bar{L}$:

$$C_{\bar{L}}^2 = \frac{(1-\beta)^2}{N_a} C_l^2 + \beta^2\left(C_p^2 + \frac{1}{N_a}\right) = 0.00186$$

The final result, expressed with a relative uncertainty of $2C_{\bar{L}}$, is

$$\bar{L} = (0.137 \pm 0.012)\ \text{mm}$$

These results are identical with those shown in Ref. 30.

Modified Point Count

The corresponding data for the modified point count method are as follows: $N_a = 1420$, $S_a = 57$, $S_t = 1000$, $S_p = 311$, and $I = 2.656$ mm

The calculation of the volume fractions is identical to that of the point count method: $A = (5.7 \pm 1.4)\%$ and $p = (31.1 \pm 2.9)\%$.

The coefficient of variation of the specific surface is

$$C_\alpha^2 = \frac{1}{S_a} - \frac{1}{S_t} + \frac{1}{N_a} = 0.0173$$

The specific surface to two standard deviations is

$$\alpha = \frac{4\,N_a}{S_a\,I}\left[1 \pm 2\,C_\alpha\right] = (37.5 \pm 9.9)\ \text{mm}^{-1}$$

As for the linear traverse method, the uncertainty in the Powers spacing factor begins with a calculation of $\bar{L}$:

$$\bar{L} = \frac{3}{4}\frac{S_a\,I}{N_a}\left[1.4\left(1 + \frac{S_p}{S_a}\right)^{1/3} - 1\right] = 0.129\ \text{mm}$$

Next, the quantity β is calculated:

$$\beta = \frac{I\,S_a}{\bar{L}\,N_a}\left(\frac{1.4}{4}\right)\left(\frac{S_p}{S_a}\right)\left(1 + \frac{S_p}{S_a}\right)^{-2/3} = 0.4570$$

The coefficient of variation in $\bar{L}$ can now be calculated:

$$C_L^2 = \frac{1}{N_a} + \beta^2 C_p^2 + (1-\beta)^2 C_{S_a}^2 = 0.00634$$

This result assumes the following:

$$C_{N_a}^2 = \frac{1}{N_a} \qquad C_{S_a}^2 = \frac{1}{S_a}$$

The final result, expressed with a relative uncertainty of $2C_{\bar{l}}$, is

$$\bar{L} = (0.129 \pm 0.021) \text{ mm}$$

Future Research

Although a thorough body of work exists on the topic of uncertainty for ASTM C 457, a number of important questions remain to be answered:

1. Monte Carlo methods could be used to demonstrate the validity of the uncertainty equations presented here. The analytical relationship between the air void radius distribution and the linear traverse chord distribution that will appear in subsequent sections can be used to choose chord lengths at random. These simulated data could then be used to estimate the various calculated quantities in ASTM C 457 and compared to the true value.
2. All of the equations presented in this section represent the smallest possible uncertainty. The equations do not account for measurement uncertainty due to finite optical resolution. The method in ASTM C 457 prescribes a minimum magnification of 50. A study is needed to determine the effects of equipment resolution.
3. A number of methods for determining the uncertainty in the paste content were proposed here. However, for someone performing a linear traverse, performing an additional test, such as a point count, to determine the paste content and its related uncertainty adds considerably to the overall effort. An alternative may be to determine information about the paste content from the air void data.
4. The assumption that the coefficient of variation in the specific surface is small should be tested using actual chord data. Also, for harmonic averages such as the specific surface, the confidence limits are not symmetric, which might have a bearing on compliance.

Inversion Formulae

There may arise situations in which the experimentalist requires information about the sphere radius distribution given information from either planar or linear probes. This is useful for the subsequent characterization of air voids in concrete containing air entrainment. This information is useful for computer simulations of an air void system[34] and studies of the effects of

the void distribution on the measured air content.[35] It is also vital to the characterization of air void spacing to be discussed in a subsequent section.

The need for accurately characterizing the air void size distribution can also arise in situations where one wishes to compare two air void distributions. The different air void distributions could arise from differences in admixture type, admixture dosage, pumping and/or atmospheric pressure, vibration, and so on. It may be useful to know how a change in the mixture proportions or the construction process affects voids of a certain size.

Although the material in this section has been thoroughly investigated for use with spherical voids, there does not appear to be a single reference for this material. The book by Underwood[14] addresses numerical procedures, but the mathematics are implied and not discussed in detail.

This section relies heavily on the use of probability density functions (PDF) and cumulative distribution functions (CDF). Since notations vary among authors, Appendix B contains an explanation of the ideas used here, along with the corresponding notation.

Definitions

There does not appear to be a single nomenclature used for the development of the subsequent equations. For clarity, the following notation will be used:

x: sphere diameter
$f(x)$: sphere diameter probability density function
$F(x)$: sphere diameter cumulative probability function
y: circle diameter : circle diameter probability density function
$g(y)$: circle diameter cumulative probability function
z: chord length
$h(z)$: chord length probability density function
$H(z)$: chord length cumulative probability function

A number of the references given in this section use sphere and circle radii and half chord lengths in their theoretical developments. The choice of radius distributions seems natural given that the equations for expectations of surface areas and volumes are more easily recognizable. However, this naturally leads to the use of the half chord length, which seems awkward. Here the use of the diameter distributions and the chord length distributions are used because concrete petrographers have experience with chord length distributions and because the relationship among sphere diameters, circle diameters, and chord lengths is somewhat intuitive.

Spheres – Circles

For the case of spheres distributed throughout a volume, a random plane will intersect the spheres, creating circles on the plane. Given a known sphere diameter distribution $f(x)$, the circle diameter distribution $g(y)$ observed on the plane was originally derived by Wicksell,[36] and subsequently derived more rigorously by Nicholson,[37] Tallis,[32] and Watson,[38]

$$g(y) = \frac{y}{\langle X \rangle} \int_y^\infty \frac{f(x)}{\left(x^2 - y^2\right)^{1/2}} \, dx \tag{41}$$

and also appears elsewhere.[7,39] Note that only the spheres with diameters greater than y contribute to the integral. This equation is based on the model-based approach of assuming the centers of the spheres constituted a Poisson process, which is correct only for a highly dilute system. Jensen[40] used a design-based approach, which simply assumes the intersecting plane is randomly oriented, to derive the same equation.

Subsequent analyses of the Wicksell problem have shown that the Wicksell equation is valid under a wide variety of conditions. Mecke and Stoyan[41] used a marked Poisson process model to demonstrate that the Wicksell equation is valid under dense conditions. The only requirement is that the centers of the spheres are stationary under translations (randomly distributed with no preferred orientation). The derivation of Cruze-Orive[42] relaxed the condition of randomness on the sphere centers and showed that Wicksell's equation is valid for any arbitrary deterministic positions and particle sizes. Therefore, no matter how the non-overlapping spheres are placed, Wicksell's equation still holds. However, inhomogeneities in the system will require additional sampling to ensure precise estimates of the particle size distribution.

The more practical problem is to determine the sphere diameter distribution from the circle diameter distribution observed on the random plane. Using an intermediate function f_1 defined by $f(x) = xf_1(x^2)$, the Wicksell equation can be rewritten as

$$g(y) = \frac{y}{2\langle X \rangle} \int_{y^2}^\infty \frac{f_1(w)}{\left(w^2 - y^2\right)^{1/2}} \, dw \tag{42}$$

This is the form of the Abel integral equation.[43,44]

The inversion has been demonstrated by Watson.[38] Multiplying Eq. 41 by $(y^2 - w^2)^{1/2}$ and integrating y from w to infinity gives

$$1 - F(w) = \frac{2\langle X\rangle}{\pi}\int_w^\infty \frac{g(y)}{\left(y^2 - w^2\right)^{1/2}}\,dy \tag{43}$$

which can be found in Wicksell[6] and Kendall and Moran.[39] In the limit where w approaches zero gives

$$1 = \frac{2\langle X\rangle}{\pi}\int_0^\infty \frac{g(y)}{y}\,dy \tag{44}$$

Therefore, the inversion equation for the sphere diameter CDF can be expressed as

$$1 - F(x) = \frac{\displaystyle\int_x^\infty \frac{g(y)}{\left(y^2 - x^2\right)^{1/2}}\,dy}{\displaystyle\int_0^\infty \frac{g(y)}{y}\,dy} \tag{45}$$

This equation is reported in Tallis[32] and Watson.[38]

The inversion equation for the sphere diameter PDF can be determined either from direct differentiation[45]:

$$f(x) = \frac{-2\langle X\rangle}{\pi}\frac{d}{dx}\int_x^\infty \frac{g(y)}{\left(y^2 - x^2\right)^{1/2}}\,dy \tag{46}$$

or from the solution to Abel's integral equation:

$$f(x) = \frac{-2\,x\langle X\rangle}{\pi}\int_x^\infty \left(y^2 - x^2\right)^{-1/2}\frac{d}{dy}\left[\frac{g(y)}{y}\right]dy \tag{47}$$

For completeness, Reid[7] reported yet another expression:

$$f(x) = \frac{1}{\pi\,x}\int_\infty^x \frac{y}{\left(y^2 - x^2\right)^{1/2}}\frac{d}{dy}\left[g(y)\right]dy \tag{48}$$

It is important to note that the circle diameter distribution on the plane cannot be monosized. The differential in the integrand would be zero except at the value of the single circle diameter. At this point the integrand is undefined. This is a mathematical reflection of the fact that it would be impossible for a random plane to intersect a collection of spheres and for all the circles on that plane have the same diameter.

Spheres – Chords

One of the earliest developments of an analytical relationship between air void diameters and chords measured along lines on a random plane is due to Reid.[7] Using similar arguments to the development of the equation relating circle diameters to sphere diameters, the chord length distribution can be calculated from the sphere distribution using the following equation[7,37,38,39]:

$$h(z) = \frac{2\,z}{\langle X^2 \rangle} \int_z^\infty f(x)\,dx \tag{49}$$

There are two important features of Eq. 49: the slope and the curvature of $h(z)$ near the origin. The slope can be determined through differentiation:

$$\frac{d}{dz} h(z) = \frac{2}{\langle X^2 \rangle}\left[1 - F(x)\right] - \frac{2\,z}{\langle X^2 \rangle} f(z) \tag{50}$$

Near the origin ($z \rightarrow 0$), the slope of the chord length distribution approaches a constant value of $2/\langle X^2 \rangle$. Since the chord PDF must be linear near the origin, the lognormal chord distribution used by Roberts and Scheiner[46] is unphysical because it has zero slope at the origin.

Differentiating Eq. 49 again gives the curvature:

$$\frac{d^2}{dz^2} h(z) = \frac{-4\,f(z)}{\langle X^2 \rangle} - \frac{2\,z}{\langle X^2 \rangle} \frac{d}{dz} f(z) \tag{51}$$

As a practical consideration, the stability of air voids assures that $f(x \rightarrow 0) = 0$. Given this fact, the chord distribution has no curvature at the origin. As the value of x increases, the curvature remains negative until after the derivative of $f(z)$ becomes negative at the modal sphere diameter. Therefore, the curvature of the chord length distribution must remain negative until z is greater than the model sphere diameter.

The derivation of the inversion equation can be seen by first rearranging Eq. 49:

$$\frac{h(z)}{z} = \frac{2}{\langle X^2 \rangle}\left[1 - F(z)\right] \tag{52}$$

The inverse of Eq. 49 can be determined from differentiating Eq. 52 with respect to z and using a change of variables to x:

$$f(x) = \frac{-\langle X^2 \rangle}{2} \frac{d}{dx}\left[\frac{h(x)}{x}\right] \tag{53}$$

As for the circles on the plane, it is impossible to have a monosized chord distribution along a random linear probe through a collection of spheres.

Circles – Chords

As a matter of completeness, the relationship between the circle diameter and the chord length distributions are given, even though this information is not currently used by ASTM C 457. The chord length distribution expressed as a function of the circle diameter distribution was reported by Reid[7]:

$$h(z) = \frac{z}{\langle Y \rangle} \int_z^\infty \frac{g(y)}{\left(y^2 - z^2\right)^{1/2}}\, dy \tag{54}$$

Since this equation is identical to the expression for $f(x)$ as a function of $g(y)$, the inversion formula can be derived in exactly the same manner:

$$g(y) = \frac{-2\langle Y \rangle}{\pi} \frac{d}{dy} \int_y^\infty \frac{h(z)}{\left(z^2 - y^2\right)^{1/2}}\, dz \tag{55}$$

Reconstruction

Reconstruction of the air void radius distribution can be accomplished using either parametric or nonparametric techniques.

Parametric

Using the parametric approach, the researcher starts with an air void radius distribution such as monosized, lognormal, Rayleigh, and so on. The probe data are then used to determine the parameters of the distribution chosen.

A parametric reconstruction reduces the problem to that of only trying to determine the moments of the distribution. Starting with some PDF for $f(x)$,

one can solve for the analytical form for the probe data distribution and the associated moments. These moments will be a function of the PDF parameters, leading to a linear system of equations. The following section is devoted to this endeavor.

Nonparametric

The nonparametric approach makes no assumptions about the analytical form for $f(x)$. The probe data are integrated numerically to give a discrete version of $f(x)$. This approach gives the "true" $f(x)$, but the data also contain noise that must be controlled. This subject is complicated and warrants its own chapter. The reader will find useful discussions in Underwood[14] and in the proceedings publications of Elias[47] and DeHoff and Rhines.[48]

Future Research

Given the small body of research performed on the analysis of air void distributions in concrete, the field remains quite fertile.

1. A parametric approach to estimating the chord distribution seems like a profitable approach to air void characterization. However, until in situ measurements of air void radii can be performed, the experimentalist will have to choose a distribution for the air void radii. One could study the effects of guessing wrong by starting with a distribution for the air void radii, choosing a different distribution to approximate it, and then comparing the approximated distribution to the original distribution.
2. A simple parametric test of the lognormal distribution can be made by measuring the first three moments of a chord distribution and determine whether or not a lognormal sphere distribution exists that has a corresponding chord distribution with nearly the same three moments.

Estimating Sphere Diameter Moments

In some cases, knowledge of the specific sphere diameter distribution may be extraneous. Rather, many calculations require only knowledge of certain expectations, such as the average sphere radius or average sphere volume, from the sphere diameter distribution. The calculation of these expectations, referred to here as moments, is discussed in detail in Appendix B.

Useful information can be gained from only making a study of the

moments of the sphere distribution. For example, the air void specific surface depends upon the ratio $\langle X^2 \rangle / \langle X^3 \rangle$. This technique has been employed in ASTM C 457. However, difficulties do exist. For planar probes, the moments $\langle X^n \rangle$ can be calculated from the averages $\overline{Y^n}$. But for linear probes, the moments can only be approximated from the averages $\overline{Z^n}$. Regardless, analysis of the moments of probe data facilitates parametric studies since one needs to solve only a linear system of equations.

Planar Probe

The straightforward means to determine the moments of the circle diameter distribution is by direct evaluation of the inversion equation[36,39]:

$$\langle Y^n \rangle = \frac{1}{\langle X \rangle} \int_0^\infty y^{n+1} \int_y^\infty \frac{f(x)}{\left(x^2 - y^2\right)^{1/2}} \, dx \, dy \tag{56}$$

The concise expression for the moments is given by Watson[38]:

$$\langle Y^n \rangle = \frac{\sqrt{\pi}}{2} \frac{\Gamma\left\{\frac{1}{2}(n+2)\right\}}{\Gamma\left\{\frac{1}{2}(n+3)\right\}} \frac{\langle X^{n+1} \rangle}{\langle X \rangle} \tag{57}$$

A more useful form for the equation is found in Wicksell[36] and in Kendall and Moran[39]:

$$\langle Y^n \rangle = \begin{cases} \dfrac{\langle X^{n+1} \rangle}{\langle X \rangle} \dfrac{1 \cdot 3 \cdot 5 \cdots n}{2 \cdot 4 \cdot 6 \cdots (n+1)} \dfrac{\pi}{2} & n \ \ is \ \ odd \\ \dfrac{\langle X^{n+1} \rangle}{\langle X \rangle} \dfrac{2 \cdot 4 \cdot 6 \cdots n}{1 \cdot 3 \cdot 5 \cdots (n+1)} & n \ \ is \ \ even \end{cases} \tag{58}$$

These equations are valid for $n \geq -1$. The equation for the harmonic mean ($n = -1$) gives a direct relationship between a single circle diameter moment and a sphere diameter moment:

$$\langle Y^{-1} \rangle = \frac{\pi}{2 \langle X \rangle} \tag{59}$$

From this, the moments with positive exponents of the sphere diameter distribution can be calculated directly from the measured circle diameter moments. The first three moments of the sphere diameter distribution are as follows:

$$\langle X \rangle = \frac{\pi}{2} \frac{1}{\langle Y^{-1} \rangle}$$
$$\langle X^2 \rangle = 2 \frac{\langle Y \rangle}{\langle Y^{-1} \rangle}$$
$$\langle X^3 \rangle = \frac{3\pi}{4} \frac{\langle Y^2 \rangle}{\langle Y^{-1} \rangle} \tag{60}$$

Specific Surface Area

The specific surface area is the ratio of the expected sphere area to the expected sphere volume:

$$\alpha = \frac{\pi \langle X^2 \rangle}{\frac{\pi}{6} \langle X^3 \rangle} = \frac{16}{\pi} \frac{\langle Y \rangle}{\langle Y^2 \rangle} \tag{61}$$

Number Density

The number density of air voids (number of voids per unit volume) n is the ratio of the air volume fraction to the expected air void volume:

$$n = \frac{A}{\frac{\pi}{6} \langle X^3 \rangle} = \frac{8A}{\pi^2} \frac{\langle Y^{-1} \rangle}{\langle Y^2 \rangle} \tag{62}$$

This equation is referred to by Watson[38] as Fullman's formula.[49] The variance in the estimate of n is proportional to the variance in the quantity $\langle Y^{-1} \rangle$, which is infinite.[32] Therefore, estimates of n from planar data may be plagued by difficulties in controlling uncertainties.

Linear Probe

In a manner similar to the planar probe, the linear probe moments can be calculated from the inversion integral:

$$\langle Z^n \rangle = \frac{2}{\langle X^2 \rangle} \int_0^\infty z^{n+1} \int_z^\infty f(x)\, dx \tag{63}$$

The solution has been reported by Wicksell,[36] Tallis,[32] and Watson[38]:

$$\langle Z^n \rangle = \frac{2}{n+2} \frac{\langle X^{n+2} \rangle}{\langle X^2 \rangle} \tag{64}$$

This equation is valid for all $n \neq -2$. Therefore, a set of equations for m different chord moments will have $m + 1$ different sphere moments, and the system of equations is underdetermined. At best, only ratios of sphere moments can be determined from chord moments.

Specific Surface Area

Fortunately, the specific surface area α is a ratio of sphere diameter moments. Therefore, it can be estimated directly from chord moments:

$$\alpha = \frac{\pi \langle X^2 \rangle}{\frac{\pi}{6} \langle X^3 \rangle} = \frac{4}{\langle Z \rangle} \tag{65}$$

This is the equation for specific surface area that is used in the ASTM C 457 standard test method.

Number Density

Although the number density cannot be determined precisely from the chord moments, there are techniques for making estimates of the quantity. The most popular has been given by Lord and Willis,[50] Watson,[38] and Philleo.[8] The approach begins with Eq. 49:

$$\frac{h(z)}{z} = \frac{2}{\langle X^2 \rangle} [1 - F(z)] \tag{66}$$

As $z \rightarrow 0$, the left side of the equation approximates the derivative of the chord distribution at the origin:

$$\left. \frac{dh}{dz} \right|_{z \rightarrow 0} = \frac{2}{\langle X^2 \rangle} \tag{67}$$

For practical reasons, the value of z does not have to equal zero. Since the air voids are thermodynamically unstable below some minimum sphere diameter x_m, the above equation is valid for all z less than x_m. Philleo[8] noted that by tabulating chord lengths smaller than x_m into the first two or three chord length intervals, each of the intervals should have an equal value of $h(z)/z$.

Calculating the slope from the smallest chord length intervals is complicated by two factors: the smallest chord length interval typically has relatively few chords, and the measurement device has a limited resolution. The small number of chords in the interval can lead to excessive statistical uncertainty. The matter of equipment resolution has been addressed by Nicholson,[37] who concluded that an unbiased estimate of the sphere number density could not be achieved with a nonzero resolution limit apparatus.

Thin Section Analysis

A recent article by Aarre[51] suggests that there is interest in quantifying an air void distribution using transmitted light through a thin section of concrete. The process consists of placing a thin section over a light source and performing a linear traverse over the specimen, recording the locations where light passes through the specimen. This approach could simplify the task of automating a linear traverse. The drawback of the technique is that the analysis of the results is more complicated than the results from a plane polished section.

The thickness of the specimen determines the diameter of the smallest air void that is detectable. Since the modal diameter of entrained air voids may be as small as 30 μm, useful specimens must be thinner than this. As an analogy, consider trying to estimate the diameter distribution of voids in Swiss cheese from thick slices from the block of cheese.

A straightforward solution to the "Swiss cheese" problem has been presented by Coleman.[52] While others have developed nonparametric techniques for unfolding the distribution, the work of Coleman gives an analytical relationship between the observed circle diameter distribution and the sphere diameter distribution, given the specimen thickness. Further, his derivation included parameters to account for the effects of resolution that include the smallest measurable circle diameter and the accuracy with which one can determine the location of the circle's edge. However, these resolution considerations will not be discussed here.

The development of the thin section equation is quite similar to that of the corresponding inversion equation for a plane polished section. For a thin section of thickness τ, only the spheres with diameters greater than τ can penetrate the thin section. Also, for each diameter, there is a volume over which the sphere center can be located and still penetrate both sides of the thin section; larger spheres have a greater volume over which their centers can be located as compared to smaller spheres. This "weights" the original sphere diameter distribution $f(x)$, and gives an adjusted distribution $m(x)$ that characterizes the distribution of the penetrating spheres[52]:

$$m(x) = \frac{(x-\tau)\, f(x)}{\int_{\tau}^{\infty} (x-\tau)\, f(x)\, dx} \tag{68}$$

The denominator normalizes the distribution and can be expressed using a shorthand notation:

$$\langle X \rangle_{\tau} = \int_{\tau}^{\infty} (x-\tau)\, f(x)\, dx \tag{69}$$

The radius of the circle Y projected through the thin section depends upon the distance W the sphere center is located from the center of the thin section:

$$Y^2 = x^2 - (W+\tau)^2 \tag{70}$$

From this, one can calculate the probability of an exposed circle with diameter Y:

$$P\left(Y > y|x\right) = P\left(W < \left(x^2 - y^2\right)^{1/2} - \tau \,\middle|\, x\right) \tag{71}$$

Because the centers of the spheres are located at uniformly random distances from the center of the thin section, the distribution of W is uniform over the interval $[x-\tau]$. Using this, the previous probability can be expressed directly:

$$P\left(Y > y|x\right) = \frac{\left(x^2 - y^2\right)^{1/2} - \tau}{x-\tau} \qquad 0 \le y \le \left(x^2 - \tau^2\right)^{1/2} \tag{72}$$

The conditional dependence upon x can be eliminated by integration:

$$P(Y > y) = \int_{\tau}^{\infty} P(Y > y|x)\, m(x)\, dx \tag{73}$$

The resulting circle diameter distribution $g_\tau(y)$ projected through the thin section is the differential of this probability function[52]:

$$\begin{aligned} g_\tau(y) &= \frac{-d}{dy} P(Y > y) \\ &= \frac{y}{\langle X \rangle_\tau} \int_{(y^2+\tau^2)^{1/2}}^{\infty} \frac{f(x)}{(x^2 - y^2)^{1/2}}\, dx \end{aligned} \tag{74}$$

In the limit that τ approaches zero asymptotically, this equation becomes identical to Eq. 41 for the plane polished section. Similarly, the nth moment for the observed circle diameter distribution can be calculated by integrating the above inversion equation:

$$\langle Y^n \rangle_\tau = \frac{1}{\langle X \rangle_\tau} \int_0^{\infty} y^{n+1} \int_{(y^2+\tau^2)^{1/2}}^{\infty} \frac{f(x)}{(x^2 - y^2)^{1/2}}\, dx\, dy \tag{75}$$

Again, as $\tau \to 0$, this equation becomes identical to the corresponding plane section equation.

Monosized Sphere Diameters

Consider a monosized sphere diameter distribution: $f(x) = \delta(x - x_0)$. (A discussion of the Dirac delta function is given in Appendix C.) Assuming that the sphere diameter x is greater than the thin section thickness τ, the observed circle diameter distribution can be calculated from Eq. 74:

$$g_\tau(y) = \frac{y}{(x_0 - \tau)} \frac{1}{(x_0^2 - y^2)^{1/2}} \qquad 0 \le y \le (x_0^2 - \tau^2)^{1/2} \tag{76}$$

The moments of this distribution can be calculated from the following integral:

$$\langle Y^n \rangle_\tau = \frac{1}{(x_0 - \tau)} \int_0^{\sqrt{x_0^2 - \tau^2}} \frac{y^{n+1}}{(x_0^2 - y^2)^{1/2}}\, dy \tag{77}$$

This result is useful for exploring the results of the paper by Aarre[51] and the subsequent discussion by Snyder.[53] The purpose of the paper by Aarre was to calculate "correction" factors when measuring air content from a thin section. The calculations assumed a monosized air void diameter distribution. The original paper by Aarre contained errors that were corrected in the discussion by Snyder.

Although the equations by Snyder were correct, they contained a subtle oversight. Let the air void diameter distribution be expressed as a Delta function, as was done in the paragraphs above. Using planar probes on a plane polished section, the air content is a function of the number of voids per unit area n and the second moment of the circle diameters measured on the plane ($\tau = 0$):

$$A = n\pi \langle Y^2 \rangle \tag{78}$$

However, an analysis of a thin section with thickness $\tau \neq 0$ will contain fewer observed voids n_τ and a different second moment $\langle Y^2 \rangle_\tau$:

$$A_\tau = n\pi \langle Y^2 \rangle_\tau \tag{79}$$

The number density of circles n observed on the plane is proportional to the first moment $\langle X \rangle$ of the sphere diameters x:

$$\int_0^\infty x\, f(x)\, dx = x_0 \tag{80}$$

The number density n_τ of circles observable through a thin section is proportional to the corresponding first moment of observable spheres $\langle X \rangle_\tau = (x_0 - \tau)$, as was defined previously. The ratio of the number density of spheres observed through thin section to the number density circles on a plane section can be expressed as a function of the thin section thickness τ:

$$\frac{n_\tau}{n} = \frac{x_0 - \tau}{x_0} = \left(1 - \frac{\tau}{x_0}\right) \tag{81}$$

The ratio of the observed air content to the true air content can now be expressed as a function of thin section thickness τ:

$$\frac{A_\tau}{A} = \frac{n_\tau \langle Y^2 \rangle_\tau}{n \langle Y^2 \rangle}$$
$$= \left[1 - \frac{3}{2}\left(\frac{\tau}{x_0}\right) + \frac{1}{2}\left(\frac{\tau}{x_0}\right)^3\right] \tag{82}$$

This is identical to the correction factor reported by Snyder.[53] However, in the derivation of Snyder, the factor of $(1 - \tau / x_0)$ was implicit in the averaging used. This factor is absent from the correction factor for specific surface because the $\langle Y^2 \rangle_\tau / \langle Y^3 \rangle_\tau$ ratio cancels this. Therefore, the result of Snyder for the specific surface is also correct.

Lineal-Path Function

Lu and Torquato[54,55] have derived the lineal-path function that gives the probability that a line segment of length τ is entirely within a single phase of the microstructure. Equivalently, this is the area fraction of light passing through a section of concrete with thickness τ. Interestingly, the lineal-path function $L(\tau)$ can be calculated from the chord length distribution function $h(z)$ and the volume fraction of air A[55]:

$$L(\tau) = \frac{A}{\langle Z \rangle} \int_\tau^\infty (z - \tau)\, h(z)\, dz \tag{83}$$

The lineal-path function for a lognormal distribution of air void radii with a modal diameter of 30 μm and with $\sigma_0 = 0.7362$ is shown in Fig. 3.

For monosized spheres of diameter x_0, the chord distribution is $h(z) = 2z / x_0^2$. Substituting this into the previous equation yields the same correction factor as given above for monosized spheres. Conversely, the chord length distribution function can be derived from air volume fraction A and the lineal-path function $L(z)$ by differentiating this equation twice:

$$h(z) = \frac{\langle Z \rangle}{A} \frac{d^2}{dz^2} L(z) \tag{84}$$

This could be applied to a serial sectioning approach to automated air void analysis using transmitted light. If the only illumination was from below the specimen, the total transmission is equivalent to $L(z)$. Therefore, a single light intensity measurement could be made at each specimen thickness and the chord length distribution could calculated from the equation above.

Future Research

Relatively little research has been carried out on thin section analysis of air voids. Given that one could determine the chord distribution $h(z)$ using a single light intensity measurement after consecutive stages of a serial section, there are possibilities for automation. However, a number of theoretical studies could be performed to validate the approach and to test the applicability of the method in general:

1. Assuming a lognormal distribution of air void radii, determine the correction factor for air content, specific surface, and spacing factor from the parameters of the distribution and the thickness of the thin section.
2. Use the formulae in Coleman[52] to determine the effect of resolution limits on the results of an analysis. These formulae could also be used to analyze resolution limits on plane section analysis.

Air Void Spacing

One of the first attempts to characterize the "spacing" of air voids was by Powers.[3] This definition of spacing became a part of the standard test method for determining the air void parameters in hardened concrete (ASTM C 457),[1] and is quantified as the spacing factor $\overline{L}$. Since then, spacing equations have been proposed by Philleo,[8] Fagerlund,[9] Attiogbe,[11] and Pleau and Pigeon.[10] Each of these equations attempts to characterize the spacing of voids in air-entrained concrete, even though the Attiogbe equation estimates the spacing among air voids, and the other equations estimate the distance water must travel to reach the nearest air void.

At present, evaluation of an air void spacing equation consists of a comparison between the estimate of spacing and the results of laboratory freeze-thaw experiments.[56,57] The a priori assumption is that each equation is inherently correct in its estimate of spacing. Unfortunately, each of these spacing equations proposed for predicting freeze-thaw performance has inherent assumptions or simplifications built into its development. Until recently, no quantitative measure has been made of the effects due to these assumptions.

A numerical accuracy test of these equations was performed by Snyder.[12] The computer experiment measured various spacing quantities in a simulated paste-air system. Systems were composed of air voids with either monosized or lognormally distributed radii. Since the size and the location of each sphere were known exactly, the actual spacings could also be calculated numerically. To achieve acceptable statistics, the results from many system

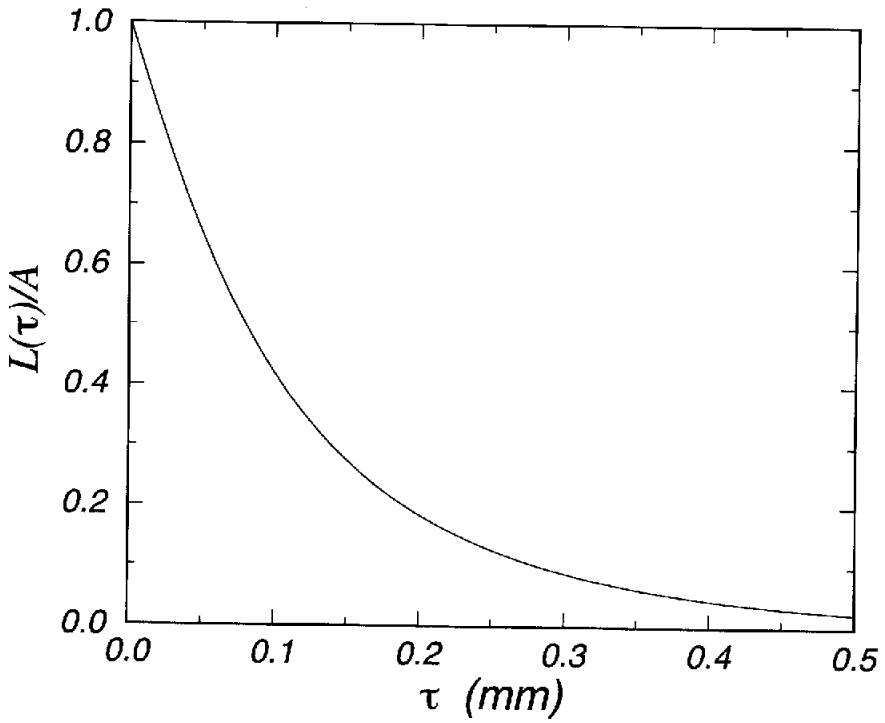

Figure 3. Lineal-path function $L(\tau)$, normalized by the air content A, for a lognormal radius distribution with a modal diameter of 30 μm and with $\sigma_0 = 0.7362$.

realizations were used to estimate averaged quantities. These results, along with the associated spacing equation predictions, were reported for comparison. In addition, an equation by Lu and Torquato[54] was included since it promised excellent performance for estimating various spacing quantities.

Spacing Distributions

This section also makes use of the ideas of probability density functions (PDF) and cumulative distribution functions (CDF), the details of which are discussed in Appendix B.

There are two classifications of spacing equations that will be discussed here. Some equations estimate the proximity of the paste to the voids, and others estimate the proximity of the voids to one another. Although this may seem a subtle distinction, it will be shown that the mathematical relationships that characterize these concepts have different behaviors.

Any reasonable concept of spacing should address the fact that there must exist a distribution of distances that characterize the spacing. Clearly, some regions of the paste are closer to an air void than other regions, and some voids have nearer neighbors than others. This characteristic can be represented by a distribution of distances, as depicted in Fig. 4 for a distance parameter s. This PDF represents the fraction of spacings found in the interval $[s,s + ds]$for some differential element ds. The CDF increases monotonically from zero to unity and represents the fraction of spacings less than s.

To illustrate the usefulness of the CDF, Fig. 4 shows two horizontal dashed lines intercept the ordinate axis at the 50th and 95th percentiles. These lines intercept the CDF at s values of 1.95 and 3.1, respectively; 50% of the spacings are less than 1.95, and 95% are less than 3.1. In theory, the CDF only asymptotes to unity; thus, to capture all of the spacings, s must increase to infinity. In practice, however, the quantity s can only increase to the size of the system. Therefore, the concept of a maximum spacing is an ill-defined quantity. Instead, a particular percentile must be chosen. In the report, the 50th and 95th percentiles of the spacing distributions were used to characterize both the measured and the estimated values, since these percentiles are intuitive to one's concept of spacing and protected paste.

Paste-Void Proximity

Paste-void proximity equations estimate the volume fraction of paste within some distance from the surface of the nearest air void. There are two simple ways to visualize this spacing, both shown schematically in Fig. 5:

1. Imagine surrounding each air void with a shell of thickness s. These shells may overlap one another, but may not overlap or penetrate air voids. The volume fraction of the paste that is within any shell is equivalent to the volume fraction of paste within a distance s of an air void surface.
2. Given an air void system, pick points at random throughout the paste that lie outside the air voids. For each point, find the distance to the nearest air void surface. The number fraction of the points that fall within a distance s of an air void surface is equal to the volume fraction of paste within a distance s of an air void surface. This second approach is the one used here to estimate the CDF of the spacing distribution.

This definition of the paste-void proximity distribution is the same as that used by proponents of the protected paste volume (PPV) concept.[58–60] The

material parameters of the concrete determine the limiting spacing, and one wants to determine the fraction of paste within this distance to the nearest air void.

Void-Void Proximity

Void-void proximity spacing equations can be further classified into either nearest neighbor or mean free path calculations.

Nearest Neighbor

Nearest neighbor void-void proximity equations estimate the surface-surface distance between nearest neighbor air voids. This idea is shown schematically in Fig. 6(a). This distance is calculated by starting from a given air void and finding the shortest distance from the surface of that void to the surface of any other air void. This is repeated for a number of different air voids. This collection of random distances, when sorted and plotted versus its relative rank, form an estimated void-void proximity cumulative distribution function.

As will be demonstrated subsequently, void-void proximity spacings have a subtle complexity. For an air-void system composed of poly-dispersed sphere diameters, the average void-void spacing originating from large spheres is smaller than the average void-void spacing originating from small spheres. Therefore, the "mean void-void spacing" is an ill-defined quantity when stated without additional qualifiers, since it varies over the distribution of sphere diameters.

Mean Free Path

The mean free path is the average length of paste between adjacent air voids along a randomly chosen line passing through the air void system, and is shown schematically in Figure 6(b). If an ASTM C 457 linear traverse was performed on a paste specimen containing entrained air voids, the mean free path would be equal to the average paste chord length. It is important to note that this distance is neither the longest nor the shortest distance between air voids in an air void system.

Aggregate Effect

The effect aggregates have on the spacing distribution has been neglected for each of the spacing equations. The assumption is that the inter-aggre-

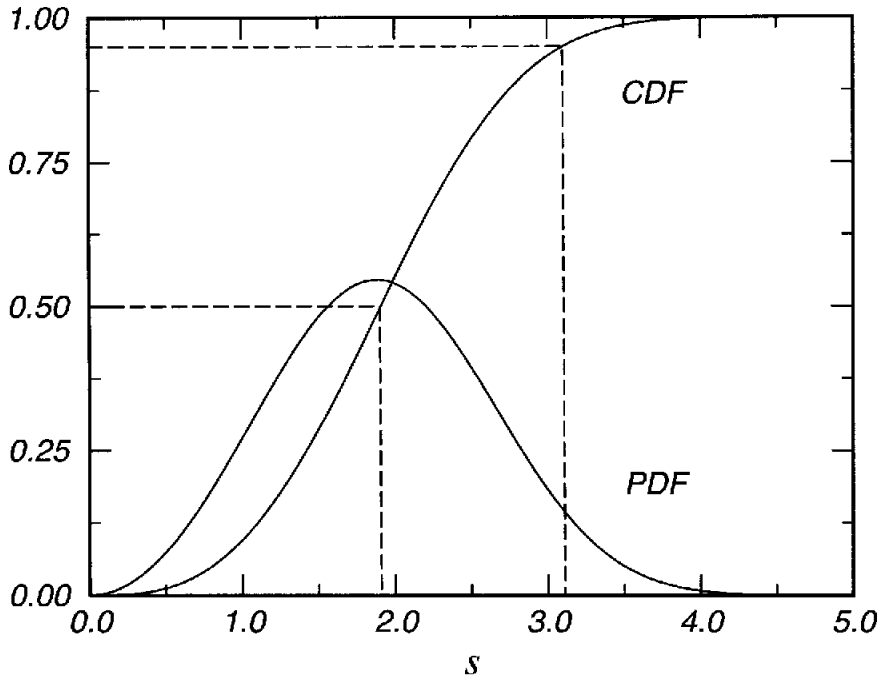

Figure 4. An idealized representation of a spacing cumulative distribution function (CDF) and the associated probability density function (PDF) for some distance s. The dashed lines demonstrate how to determine the 50th and 95th percentiles from CDF data.

gate paste regions are large enough to contain a statistically significant number of air voids. Based upon this assumption, the statistics calculated for the air voids in these inter-aggregate regions are unbiased estimates of the values calculated from the paste-air systems with the same number density of air voids. Measurements by Diamond et al.[61] indicate that the average inter-aggregate spacing on a plane section is on the order of 100 μm. Since this spacing in three dimensions may be less, the presence of aggregates may have a significant impact on spacing since there may only be a few air voids within many of the inter-aggregate regions. However, recent results by Bentz and Snyder[62] suggest that the effect upon relevant statistical properties due to aggregates is negligible if the aggregates are larger than the air voids of interest. Although further study is needed, this paper neglects the effect of aggregates, as do most air void spacing equations.

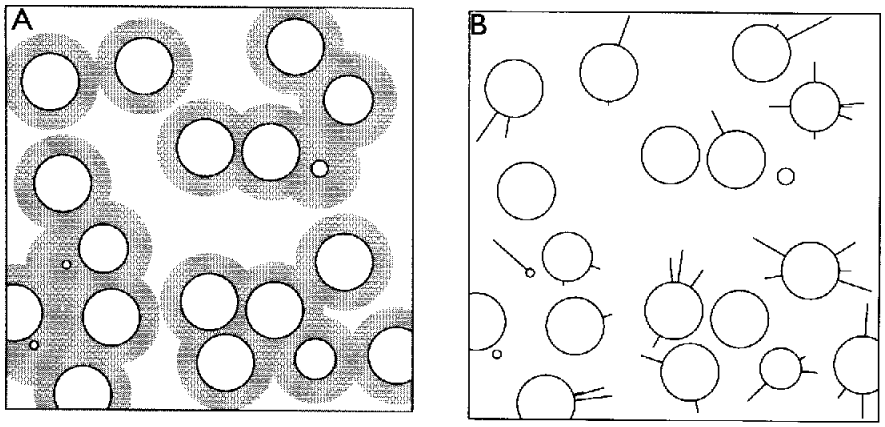

Figure 5. Two-dimensional schematic of the paste-void proximity. The quantity can determined from the volume of concentric shells (a) or from the nearest surface distance distribution (b).

Spacing Equations

Nomenclature for air void quantities differs among various authors. To express quantities with a common notation here, the following definitions are given:

- n: number of air voids per unit volume
- A: air void volume fraction
- p: paste volume fraction
- α: specific surface area of voids
- r: sphere radius
- $f(r)$: sphere radius probability density function
- $\langle R^k \rangle$: expectation of R^k for the radius distribution
- s: spacing distribution parameter

For the paste-air systems (no aggregate) considered here, these quantities can be defined analytically as follows:

$$A = \frac{4\pi}{3} n \langle R^3 \rangle$$
$$p = 1 - A$$
$$\alpha = 3 \frac{\langle R^2 \rangle}{\langle R^3 \rangle}$$
$$\langle R^k \rangle = \int_0^\infty r^k \, f(r) \, dr \tag{85}$$

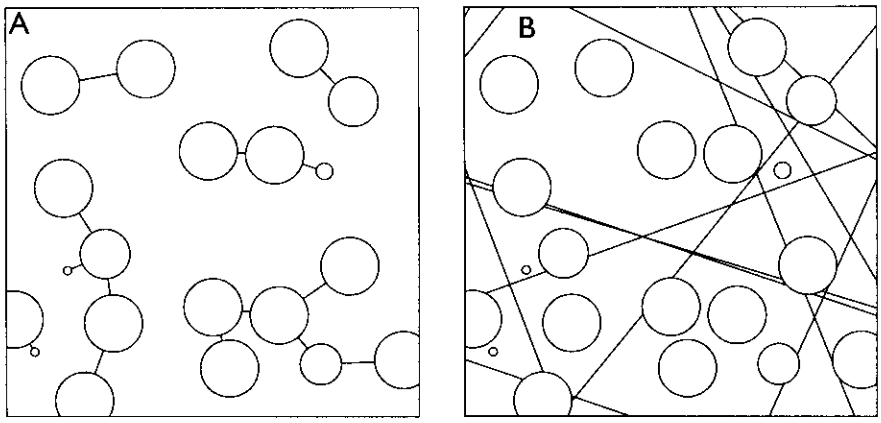

Figure 6. Two-dimensional schematic of the void-void proximity (a) and mean free path (b).

Powers Spacing Factor

The most widely used paste-void spacing equation is the Powers spacing factor.[3] Contrary to a popular misconception, it does not attempt to estimate the distance between air voids. Rather, it is an attempt to calculate the fraction of paste within some distance of an air void (paste-void proximity). The Powers equation approximates the constant distance from the surface of each air void surface, which would encompass some large fraction of the paste. However, the value of this fraction is not quantified.

The second misconception is that the Powers spacing factor represents the maximum distance water must travel to reach the nearest air void in a concrete specimen.[57,63] From the previous discussion of the distribution of paste-void and void-void spacings, it should be clear that there is no single theoretical maximum value for the paste-void spacings. One can only quantify percentiles of the distribution to characterize the fraction of paste within some distance to the nearest air void surface. In practice, the maximum paste-void spacing is the size of the sample.

The Powers spacing factor was developed using two idealized systems. For small values of the p/A ratio, there is very little paste for each air void. Powers used the "frosting" approach of spreading all of the paste in a uniformly thick layer over each air void. The thickness of this "frosting" is approximately equal to the ratio of the volume of paste to the total surface area of air voids:

$$\bar{L} = \frac{p}{4\pi\, n \langle R^2 \rangle} = \frac{p}{\alpha\, A} \qquad p/A < 4.342 \tag{86}$$

For large values of the p/A ratio, Powers used the cubic lattice model. The spheres are placed at the vertices of a simple cubic array. The air voids are monosized, each with a specific surface area equal to the bulk value. The cubic lattice spacing is chosen such that the air content equals the bulk value. The resulting Powers spacing factor is the distance from the center of a unit cell to the nearest air void surface:

$$\bar{L} = \frac{3}{\alpha}\left[1.4\left(1 + \frac{p}{A}\right)^{1/3} - 1\right] \qquad p/A \geq 4.342 \tag{87}$$

The p/A value of 4.342 is the point at which these two equations are equal.

The intent was that a large fraction of the paste should be within $\bar{L}$ of an air void surface. An acceptable value of $\bar{L}$ for good freeze-thaw performance is determined from the material properties of the concrete.

Philleo Spacing Equation

Philleo[8] extended the approach of Powers by attempting to quantify the volume fraction of paste within some distance of an air void system (paste-void proximity). Philleo started with an idealized air void system composed of n randomly distributed points per unit volume. The probability that the nearest randomly distributed point is a distance x from a random location was first given by Hertz[64]:

$$H(x) = 1 - \exp\left(\frac{-4\pi\, n}{3}\, x^3\right) \tag{88}$$

This is equivalent to the cumulative paste-void proximity distribution function for zero radius voids. Philleo then modified this distribution to account for finite-sized spheres by renormalizing the cumulative distribution to account for the air content. The rescaling is shown schematically in Fig. 7. For a void content of 0.20, the ordinate axis is rescaled from 0 to 1, and the abscissa axis is simply offset by $s = x - x_0$.

The result, although still only an approximation, characterizes the paste-void spacings for finite-sized air voids. For an air-paste system, the Philleo

spacing factor for the volume fraction of paste within a distance s of an air void surface is

$$F(s) = 1 - \exp\left[-4.19x^3 - 7.80x^2\left(\ln p^{-1}\right)^{1/3} - 4.84x\left(\ln p^{-1}\right)^{2/3}\right] \quad (89)$$

Here, the substitution $x = sn^{1/3}$ has been made in order to simplify the appearance of the result.

Fagerlund Spacing Equation

The approach used by Fagerlund[9] is similar to that of Philleo. The air void system is approximated by non-overlapping voids. Each void is surrounded by a shell with thickness s. For small air contents and small values of s, the shells are essentially non-overlapping. As the shell thickness s increases, the number of shells that intersect increases. The value of s for which half of the void shells intersect another shell is denoted $\bar{s}$. Fagerlund defines the mean void spacing $\bar{d}$ as twice this value:

$$\bar{d} = 2\,\bar{s} \quad (90)$$

To estimate $\bar{s}$, Fagerlund uses the volume v_s of the shell system:

$$v_s = \int_0^\infty f(r)\,\frac{4\pi\, n}{3}\,(r+s)^3\,dr \quad (91)$$

The value $\bar{s}$ is approximated from that value of s required to make v_s equal to unity:

$$\int_0^\infty f(r)\,\frac{4\pi\, n}{3}\left(r+\bar{s}\right)^3\,dr = 1 \quad (92)$$

This equation is simplified by expanding the cubic term and substituting for $\bar{d}$ and the specific surface area α[9]:

$$\frac{4\pi\, n}{3}\langle R^3\rangle\left[1+\left(\frac{\alpha}{2}\right)\bar{d}+\left(\frac{\alpha}{4}\right)\frac{\langle R\rangle}{\langle R^2\rangle}\,\bar{d}^2+\left(\frac{\alpha}{8}\right)\frac{1}{3\,\langle R^2\rangle}\,\bar{d}^3\right] = 1 \quad (93)$$

For an air void radius distribution $f(r)$, one simply needs to solve this cubic equation for $\bar{d}$.

Attiogbe Spacing Equation

Attiogbe has proposed a spacing equation which estimates the "mean spacing of air voids" in concrete.[11] From the figures in the paper by Attiogbe, it appears as though the spacing equation attempts to estimate one-half of the average minimum surface-surface spacing among neighboring air voids. However, an accurate numerical test of the equation is complicated by ambiguity in the exact definition of what the Attiogbe spacing equation attempts to quantify. Figure 1 of Ref. 11 depicts the spacings considered. In that figure, the author has chosen the nearest three voids as neighbors. Attiogbe should have included the other six voids that are "visible" to the central void since, by Attiogbe's definition, "$\bar{d}$ is defined by considering only the distances, between adjacent air voids, which are entirely occupied by paste."[11]

A definitive numerical test of the Attiogbe spacing equation is complicated further by a choice between two spacing equations. The first equation published was, "valid for all values of p/A"[11]:

$$t = 2\,\frac{p^2}{\alpha\, A} \tag{94}$$

To avoid confusion with the other spacing equations presented here, the variable t has been substituted for $\bar{s}$ used in the original equation. Upon noting that this equation has peculiar properties for some values of p/A,[65] Attiogbe has proposed a more complete equation[57]:

$$t_G = 2\,G\,\frac{p^2}{\alpha\, A} \tag{95}$$

The variable G replaces the variable F to avoid confusion with the Philleo spacing factor. Attogbe states that, "[G] . . . is the fraction of the total paste volume within the distances of [t] from the edges of the air voids. . . . In this regard, [G] is equivalent to the probability factor defined in Philleo's 'protected paste volume concept.'"[11] The function is only a function of the paste-to-air ratio[11]:

$$G = \begin{cases} \dfrac{8}{p/A + 1} & p/A \geq 7 \\ 1 & p/A < 7 \end{cases} \tag{96}$$

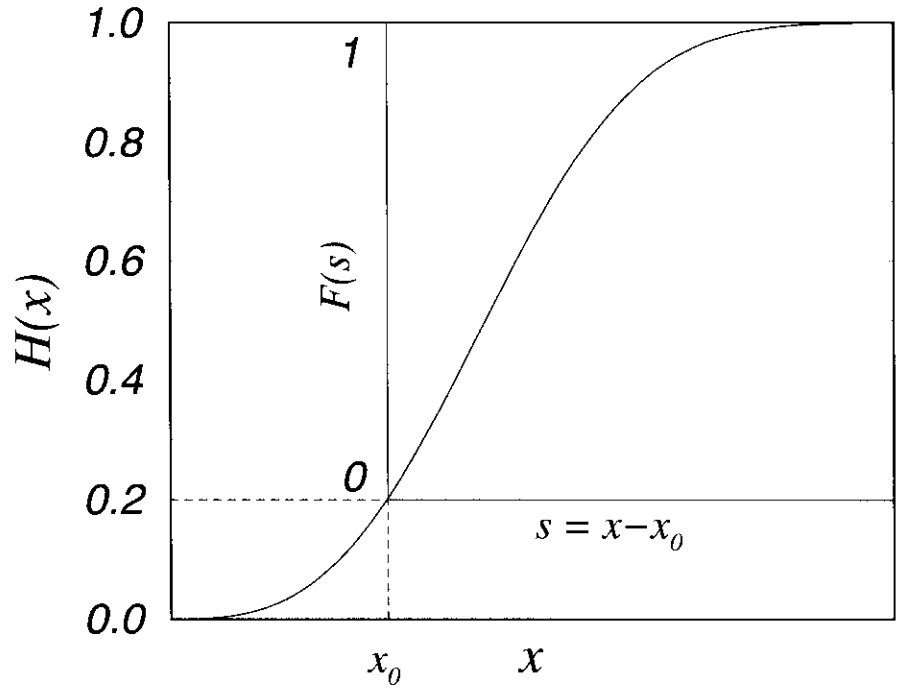

Figure 7. Schematic of Philleo method for rescaling the Hertz probability distribution function for a 20% volume fraction of voids.

However, the quantity G depends upon the air void radius distribution. Fortunately, Attiogbe[66] has recently given an explicit equation for G for an air void diameter probability density function $f(x)$ based upon the gamma function[67]:

$$f(x) = \frac{x^{a-1}\, e^{-x/b}}{b^a\, \Gamma(a)} \tag{97}$$

The parameters a and b can be related to the mean diameter $\overline{X}$ and the variance of the distribution σ^2:

$$a = \frac{\overline{X}^2}{\sigma^2} \qquad b = \frac{\sigma^2}{\overline{X}} \tag{98}$$

For any parameters (a,b), the equation for G has been given[66]:

$$G = \frac{(18/\pi)\left[1+(a+3)/4a\right]}{p/A+1} \tag{99}$$

This result can be applied to the lognormal air void radius distributions. Additionally, since G is an estimate of the fraction of paste within t of an air void, it will be compared to measured values.

Mean Free Path

The behavior of the Attiogbe function t for voids of zero radius suggested a relationship to the mean free path λ between air voids. As stated previously, the mean free path is numerically equivalent to the average paste chord lengths in a paste-air system. The probability density function of paste chords can be found in Lu and Torquato,[55] and is expressed as a function of moments of the air void radius distribution:

$$h_p(z) = \frac{n\pi\langle R^2\rangle}{1-A}\exp\left(\frac{-n\pi\langle R^2\rangle}{1-A}z\right) \tag{100}$$

This is the exponential distribution. For a paste-air system, the mean paste chord length λ can be written directly:

$$\lambda = \frac{p}{n\pi\langle R^2\rangle} \tag{101}$$

The same equation can be found in stereology books such as that of Underwood.[14] If the center of the air voids remain fixed, as the radii of the air voids decreases to zero, the mean free path diverges toward infinity, like the Attiogbe equation for t.

This similarity is more than coincidental. In fact, the Attiogbe equation for t is directly proportional to λ. Expressing the Attiogbe equation for t as

$$t = 2p\frac{p}{\alpha A} \tag{102}$$

the quantity αA can be simplified using Eqs. 85:

$$t = \frac{p}{2} \frac{p}{n\pi \langle R^2 \rangle}$$

$$= \frac{p}{2} \lambda \tag{103}$$

Therefore, at low air contents the value of t is approximately equal to one-half the mean free path between air voids in a paste-air system. It is interesting to note that the Powers equation for $p/A < 4.342$ is equal to $\lambda/4$. Therefore, at high air contents, there should be relatively little qualitative difference between the Attiogbe and the Powers equations. However, at low air contents, the two equations have different asymptotic behavior.

Pleau and Pigeon Spacing Equation

Pleau and Pigeon[10] have recently proposed a spacing equation for the paste-void spacing distribution. Their approach considers both the air void radius distribution and the distribution of distances between a random point in the paste and the nearest air void center. Let $h(x)$ represent the probability density function of the distance between a random point in the system and the center of the nearest air void. The joint probability β that this random point is a distance s from the surface of an air void with radius r is

$$\beta(s,r) = h(r + s)\, f(r) \tag{104}$$

As an approximation for $h(x)$, Pleau and Pigeon employ the PDF of the Hertz distribution[64] used by Philleo[8]:

$$h(x) = 4\pi\, n \exp\left(\frac{-4\pi\, n}{3} x^3\right) \tag{105}$$

However, the centers of air voids are not entirely random since air voids do not overlap one another. The consequence of this choice for $h(x)$ is discussed subsequently.

The joint probability density function $\beta(s,r)$ depends upon $h(s + r)$. If a point chosen at random throughout the entire system lies at a distance x from the center of a sphere, the quantity s is defined as $x - r$. Therefore, if

the random point lies within the sphere, the quantity s will be negative, but the argument x of $h(x)$ will be either zero or some positive number.

The parameter r may be eliminated from the joint probability $\beta(s,r)$ by integrating over the possible radii:

$$k(s) = \int_0^\infty h(r+s)\, f(r)\ \Theta(r+s)\, dr \tag{106}$$

The Heaviside function[68] insures that the argument of the function h remains positive. This equation is the fundamental equation of Pleau and Pigeon. The cumulative distribution function is

$$K'(s) = \int_{-\infty}^{s} k(s')\, ds' \tag{107}$$

and corresponds to the volume fraction of the entire system within s of an air void center. The volume fraction of the entire system that would lie within an air void is $K'(0)$, and corresponds to an estimate of the air void volume fraction. The volume fraction of paste within s of an air void surface would then be

$$K(s) = \frac{1}{Q}\int_0^s k(s')\, ds' \tag{108}$$

where Q normalizes the result by the volume fraction of paste.

The normalization factor Q should equal $1 - A$, or the paste volume fraction. Based upon the equations of Pleau and Pigeon, this is equivalent to

$$Q = 1 - K'(0) \tag{109}$$

which is used in their derivation. However, as demonstrated previously,[69] for monosized spheres the quantity $K'(0)$ corresponds to the air volume fraction for a system of overlapping spheres. This is a consequence of using the Hertz distribution for $h(x)$.

In the subsequent numerical experiment, two results will be reported for the Pleau and Pigeon equation corresponding to the normalization factors $1 - K'(0)$ and $1 - A$.

Lu and Torquato Equations

The paste-void and the void-void spacing distributions have application both inside the field of cementitious materials[70–75] and outside the field.[76–78]

Using various approximation techniques, the problems of the paste-void and the void-void spacing distributions have been solved for systems composed of monosized spheres.[79-85] These approximations have been compared to results of Monte Carlo method simulations[82,83] and they are in agreement. One method of approximation relies upon n-point correlation functions, and Torquato, Lu, and Rubenstein[83] have obtained exact expansions for monosized spheres. Lu and Torquato[86] developed a means to map these correlation functions to systems of polydispersed sphere radii, thereby making it possible to extend the approximations for monosized spheres. These approximations for poly-dispersed sphere radii are given in Lu and Torquato,[54] and are used here as estimates for both the paste-void and the void-void spacing distribution.

The results of Lu and Torquato[54] for both the paste-void and the void-void proximity calculations require the following defined quantities:

$$\begin{aligned}
\xi_k &= \frac{\pi}{3} n\, 2^{k-1} \langle R^k \rangle \\
c &= \frac{4\langle R^2 \rangle}{1-A} \\
d &= \frac{4\langle R \rangle}{1-A} + \frac{12\,\xi_2}{(1-\xi_3)^2}\langle R^2 \rangle \\
g &= \frac{4}{3(1-A)} + \frac{8\,\xi_2}{(1-A)^2}\langle R \rangle + \frac{16}{3}\frac{B\,\xi_2^2}{(1-A)^3}\langle R^3 \rangle
\end{aligned} \tag{110}$$

The value of B depends upon the exact way the system is constructed. For the calculations performed here, $B = 0$. Also, there was an error in the published value for g in Ref. 54, which has been corrected here.

Since Lu and Torquato were studying systems composed of a matrix containing solid spheres, they use the terms "void" and "particle" to represent the matrix and the spheres, respectively. Therefore, the Lu and Torquato "void exclusion probability" is used here to estimate the paste-void proximity distribution, and their "particle exclusion probability" is used here to estimate the void-void proximity distribution.

Paste-Void Proximity Distribution

The approach of Lu and Torquato[54] was to derive the probability that a point chosen at random throughout the entire system would have no part of an air void within a distance s from it. The region of thickness about the

point constitutes a test sphere of radius s. This test sphere of radius s constitutes the Lu and Torquato "void." This void exclusion probability is given in Ref. 54:

$$e_V(s) = \begin{cases} 1 - \dfrac{4\pi}{3} n \left\langle (s+r)^3 \, \Theta(s+r) \right\rangle & s < 0 \\ (1-A) \exp\left[-\pi \, n\left(cs + ds^2 + gs^3 \right) \right] & s > 0 \end{cases} \tag{111}$$

Having $s < 0$ corresponds to a sphere with radius $-(s)$ being entirely inside an air void. The averaged quantity in Eq. 111 has the same definition as before:

$$\left\langle (s+r)^3 \, \Theta(r+s) \right\rangle = \int_0^\infty (s+r)^3 \, \Theta(s+r) \, f(r) \, dr \tag{112}$$

This result can be recast into the air void problem. Since $e_V(s)$ represents the probability of a random point not being within a distance s of an air void surface, the probability of finding the nearest void surface within a distance s of a randomly chosen point is the complement of the void exclusion probability:

$$E'(s) = 1 - e_V(s) \tag{113}$$

The probability of finding the nearest air void surface a distance s from a random point in the paste portion requires only the air content A:

$$\begin{aligned} E_V(s) &= \frac{E'_V(s>0) - A}{1 - A} \\ &= 1 - \exp\left[-\pi \, n\left(cs + ds^2 + gs^3 \right) \right] \end{aligned} \tag{114}$$

The quantity $E_V(s)$ is the fraction of the paste volume within a distance s of an air void surface, which is equivalent to the definition of the paste-void proximity cumulative distribution function.

Void-Void Proximity Distribution

The approach used by Lu and Torquato[54] for the void-void proximity is similar to that for the paste-void proximity. For a point located at the center

of an air void with radius R, the probability that the nearest air void surface is farther away than w is given in Ref. [54]:

$$e_P(w,R) = \begin{cases} 1 & w \le R \\ \exp\left\{-\pi n\left[c\left(w-R\right)+d\left(w^2-R^2\right)+g\left(w^3-R^3\right)\right]\right\} & w > R \end{cases} \quad (115)$$

Lu and Torquato refer to this as the particle exclusion probability.

The probability that the nearest air void surface is within a distance w from the center of an air void with radius R is

$$\begin{aligned} E_P'(w,R) &= 1 - e_P(w > R, R) \\ &= 1 - \exp\left\{-\pi n\left[c\left(w-R\right)+d\left(w^2-R^2\right)+g\left(w^3-R^3\right)\right]\right\} \end{aligned} \quad (116)$$

Let s represent the shortest surface-surface distance between two air voids. The probability $E_P(s,R)$ that the nearest air void surface is within s of the surface of the void with radius R requires only a substitution of variables:

$$E_P(s,R) = E_P'(s+R,R) \quad (117)$$

The function $E_P(s,R)$ is equivalent to the void-void spacing cumulative distribution function.

The most important feature of Eq. 117 is that $E_P(s,R)$ depends upon the size of the sphere one starts from. For monodispersed sphere diameters, R is a constant. However, for a system composed of polydispersed sphere diameters, $E_P(s,R)$ is a continuous function of R. Since a continuous distribution of sphere diameters would have an infinite number of possible diameters, there would exist an infinite number of possible $E_P(s,R)$ distributions. This complicates an evaluation of void-void spacing distributions for systems composed of polydispersed sphere radii.

One possible remedy is to calculate an ensemble average. Ensemble averages can be calculated based on either number density or volume density. This bulk value can then be compared to measured values. Here, the number density ensemble average was chosen:

$$\left\langle E_P(s)\right\rangle = \int_0^\infty E_P(s,r)\, f(r)\, dr \quad (118)$$

For a system of poly-dispersed sphere diameters one can also calculate the mean nearest surface-surface distance $l_P(R)$ as a function of sphere radius R[54]:

$$l_p(R) = \int_R^\infty e_p(w, R)\, dw \tag{119}$$

This gives the average surface-surface distance to the nearest air void surface when starting from spheres of radius R. The quantity $l_p(R)$ decreases as R increases. Therefore, on average, the larger the sphere one starts from, the shorter the distance one travels to reach the surface of the nearest air void.

Numerical Test

As a measure of spacing equation accuracy on a geometrical level, a numerical experiment was conducted using air void radii from a zeroth-order logarithmic distribution[87]:

$$f(r) = \frac{\exp\left[-\frac{1}{2}\left(\frac{\ln(r / r_0)}{\sigma_0}\right)^2\right]}{\sqrt{2\pi}\,\sigma_0\, r_0 \exp\left(\sigma_0^2 / 2\right)} \tag{120}$$

Since this distribution is quite useful for parametric studies of air voids, its details are discussed in Appendix D. Some of the results from Ref. 12 are shown here in the following tables. The systems were composed of lognormally distributed air void radii with a modal radius r_0 of 15 μm, and a value of 0.736 for the dispersion parameter σ_0 (standard deviation of the logarithms).

The measured values are the average and estimated standard deviation from 100 system realizations. Each realization consisted of a fresh collection of air void radii from the lognormal distribution, and new random locations for each void. For each new system, the voids were placed sequentially, largest to smallest, such that no two voids overlapped one another.

Paste-Void Proximity

The results reproduced in Table I suggest that the Powers spacing factor approximates some large percentile of the paste-void spacing distribution, as it was intended. For the logarithmic radius distribution used here, the Powers spacing factor is approximately 150% of the 95th percentile of the paste-void proximity distribution.

The Philleo equation consistently predicts the 95th percentile of the paste-void proximity distribution to within 10% error. This is somewhat

remarkable given that it does not include information regarding the specific air void radius distribution.

The Fagerlund quantity $\bar{d}$ is meant to be an approximation, like the Powers factor $\bar{L}$. There is no a priori reason why $\bar{d}$ should predict the 95th percentile of the paste-void distribution. However, although the Fagerlund quantity $\bar{d}$ is not an accurate predictor of the 95th percentile, its ratio to the 95th percentile was also nearly constant for all the air contents tested.

The Pleau and Pigeon equation was also a reasonably accurate predictor of the 95th percentile of the paste-void proximity distribution. The value that was normalized by the air content for K_A was accurate to within 10%. The fact that the Pleau and Pigeon equation is accurate at the 95th percentile is due to the morphology of the system that contains 95% of the paste. This system would appear similar to a system of overlapping spheres, and would explain why their equation can work so well given that they assumed a system of overlapping spheres for the air void system.[13]

The Lu and Torquato estimate of the 95th percentile agreed with the measured value to within one standard deviation. It would appear as though the Lu and Torquato equation is sufficiently accurate for predicting the paste-void proximity distribution over the range of air contents expected in practice.

Void-Void Proximity

The results of the void-void proximity distribution estimates are shown in Table II. The Attiogbe equation for t is proportional to λ as expected. The Attiogbe quantity t_G is greater than the measured 50th percentile $vv50$ by at least a factor of five. Also, the value of t_G varied by a factor of three over the range of air contents, while the value of $vv50$ varied by a factor of 6. This would suggest that t_G is not proportional to $vv50$.

The Lu and Torquato estimate of the void-void distribution was based on Eq. 118. As for the paste-void proximity, the Lu and Torquato estimate of the 50th percentile of the void-void proximity distribution was within one standard deviation of the measured values, and appears to be sufficiently accurate over the range of air void volume fractions expected in concrete.

The performance of the function G in estimating the fraction of paste within t of an air void is shown in Table III. The value of G was calculated for the lognormal distribution by equating the parameters of the distribution in Eq. 97 to the statistical properties in Eq. 98. Because of the accuracy of the Lu and Torquato equations, the value given by E_V is used as a reference. The value of G varies by nearly an order of magnitude for the values of p/A

investigated. However, both $E_V(t)$ and $E_V(t_G)$ were equal to 1.000 over the same range.

The Lu and Torquato equation for E_P is an accurate estimate of the measured quantity $vv50$. The equation estimated $vv50$ to within one standard deviation over the range of air contents reported. The mean nearest surface-surface distance $l_P(R)$ for the two extreme air contents are shown in Fig. 8. The details of the numerical calculation from the simulated systems are given in Ref. 12. Once again, the Lu and Torquato equation is very accurate.

Lu and Torquato Equation

The performance of the Lu and Torquato equation is, by far, the most accurate estimate for every statistic considered. Not only does it predict these statistics well, it also predicts the average void-void spacing as a function of the radius for polydispersed sphere radii. It appears as though the Lu and Torquato equation is accurate to the level of precision required for investigations of air void spacing. These results also suggest that, at the air volume fractions investigated here, an air void distribution approximated by a collection of parked spheres has very similar spatial statistics to an equilibrium distribution of spheres, which has relevance to numerical tests of air void equations. It is also interesting to note that the Lu and Torquato equations do not require information about the entire air void radius distribution. Rather, only the values $\langle R \rangle$, $\langle R^2 \rangle$, and $\langle R^3 \rangle$ are needed.

Paste-Void Probability Density Function

A graphical performance comparison of the Philleo, the Pleau and Pigeon, and the Lu and Torquato estimates of the paste-void proximity probability density function is shown in Fig. 9. The sphere radii are lognormally distributed with a number density of 240 mm^{-3}. The Philleo estimate terminates at $s = 0$ because it is already normalized for the fraction of paste within s of an air void surface. The Lu and Torquato estimate is virtually exact at the resolution of this experiment. The Philleo estimate is fairly accurate for s greater than zero; while that of Pleau and Pigeon is noticeably in error. These qualitative differences are borne out in the previously reported results.

Analytical Test

Given the accuracy of the Lu and Torquato equations, subsequent tests of air void spacing equations can be performed without numerical simulation. Instead, the results can be compared directly to the Lu and Torquato equa-

Table 1. Estimates of the 95th percentile of the paste-void distribution for log-normally distributed sphere radii with number density *n* and air content *A*

n (mm)	A	$\bar{L}$ (mm)	F (mm)	$\bar{d}$ (mm)	K_A (mm)	$K_{K'}$ (mm)	E_V (mm)	$pv95$ (mm)
20	0.016	0.450	0.272	0.381	0.302	0.304	0.290	0.290±0.005
40	0.033	0.337	0.204	0.285	0.231	0.236	0.220	0.219±0.004
80	0.066	0.247	0.150	0.206	0.173	0.185	0.162	0.162±0.003
160	0.131	0.175	0.108	0.143	0.125	0.143	0.114	0.114±0.002
240	0.197	0.136	0.087	0.110	0.099	0.123	0.089	0.090±0.002

Table from Ref. 12. The estimates are from the equations of Powers ($\bar{L}$); Philleo (F); Fagerlund ($\bar{d}$); Pleau and Pigeon (K_A) and ($K_{K'}$); and Lu and Torquato (E_V). The measured values are labeled $pv95$ and have the one standard deviation uncertainties shown.

tion. Using this approach, a more thorough test of the spacing equations that uses a wider range of possible air void radius distributions can be investigated. The results presented here are from Ref. 13.

Air Void Radius Distributions

As was done for the numerical test, the analytical test used the zeroth-order logarithmic distribution because it was a reasonable representation of air void radii in concrete containing air entrainment. (Appendix D contains a detailed discussion of this distribution.) Figure 10 shows the distributions used in the analytical test. The distributions are plotted as a function of diameters to be more easily associated with chord lengths obtained from linear traverse.

An additional air void diameter distribution, not shown in Fig. 10, used in the study is a monosized distribution composed of 200 μm diameter spheres. The distribution corresponds to lognormal distribution parameters of $r_0 = 0.100$ mm, $\sigma_0 = 0$.

Results

The performance of the air void spacing equations was quantified by the accuracy with which they predicted the 95th percentile of the paste-void spacing distribution. The estimate of the distance at the 95th percentile s_{95} using the Lu and Torquato equation was used as a reference value, and is expressed mathematically as the inverse of the function $E_V(s)$:

$$s_{95} = E_V^{-1}(0.95) \tag{121}$$

Table II. Estimates of the 50th percentile of the void-void distribution for log-normally distributed sphere radii with number density *n*, air content *A*, and mean free path λ

n (mm^{-3})	A	λ (mm)	t (mm)	t_G (mm)	E_P (mm)	$vv50$ (mm)
20	0.016	7.969	3.919	0.642	0.134	0.134±0.003
40	0.033	3.918	1.895	0.621	0.092	0.093±0.002
80	0.066	1.892	0.884	0.580	0.060	0.060±0.002
160	0.131	0.880	0.382	0.382	0.035	0.035±0.001
240	0.197	0.542	0.218	0.218	0.024	0.024±0.001

Table from Ref. 12. The estimates are from the equations of Attiogbe (t and t_G) and Lu and Torquato (E_P). The measured values are labeled $vv50$ and have the one standard deviation uncertainties shown.

Table III. Estimates of the fraction of paste within either t or t_G of an air void surface for a lognormal air void distribution with number density *n* and air content *A*

n (mm^{-3})	A	p/A	t (mm)	t_G (mm)	G	$E_V(t)$	$E_V(t_G)$
20	0.016	59.84	3.919	0.642	0.164	1.000	1.000
40	0.033	29.42	1.895	0.621	0.328	1.000	1.000
80	0.066	14.21	0.884	0.580	0.656	1.000	1.000
160	0.131	6.605	0.382	0.382	1.000	1.000	1.000
240	0.197	4.070	0.218	0.218	1.000	1.000	1.000

Table from Ref. 12. The estimates are calculated from the Lu and Torquato equation for E_V.

The accuracy of the other spacing equations was quantified by the ratio of the spacing equation estimate to the Lu and Torquato value of s_{95}. For the Powers, Philleo, and Pleau and Pigeon equations, these ratios are, respectively:

$$Q_{\bar{L}} = \frac{\bar{L}}{s_{95}} \qquad Q_F = \frac{F^{-1}(0.95)}{s_{95}} \qquad Q_K = \frac{K^{-1}(0.95)}{s_{95}} \tag{122}$$

The results were reported as a function of the paste air content. The corresponding air contents for concrete would be approximately one-third of this value.

The values of $Q_{\bar{L}}$ for the Powers spacing equation are shown in Table IV.

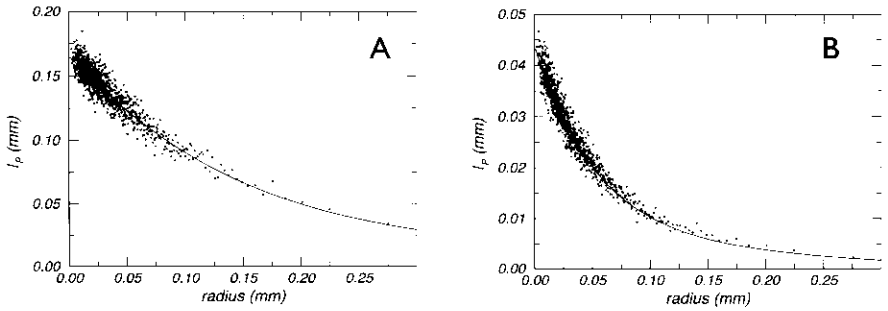

Figure 8. Mean void-void spacing l_p for lognormally distributed sphere radii with number density n: (a) 20 mm^{-3} and (b) 240 mm^{-3}. Measured values are shown as solid circles; the solid line is the estimate by Lu and Torquato. (From Ref. 12.)

The results indicate that $Q_{\bar{L}}$ for the Powers equation is a function of only the air content A and σ_0. The minimum value for $Q_{\bar{L}}$ is nearly unity for monosized spheres, and it increases to a value near two for the distributions used here. Note also that the non sequitur values for the 0.21 paste air content are due to the use of Eq. 86 as the ratio p/A becomes greater than 4.342.

Values of Q for the Philleo and the Pleau and Pigeon spacing equations are shown in Tables V and VI, respectively. These two equations have similar results. Over most of the parameter space investigated, the equations are typically within 10 % of s_{95}. Near the limits of the parameter space, the equations are still within approximately 20% of s_{95}. Also, as was true for the Powers spacing equation, the value of Q for these two spacing equations was only a function of σ_0 and A, and not a function of r_0.

The fact that all three spacing equations are only functions of σ_0 and A means that each equation can be corrected, given this information. One could perform a parametric study of linear traverse data, determine the corresponding parameters of the sphere radius distribution, and calculate σ_0. This, along with the air content A, could be used to establish an accurate estimate for s_{95}.

Upon reflection, it is not surprising that both the Philleo and the Pleau and Pigeon spacing equations can accurately predict the 95th percentile of the paste-void spacing distribution. As seen in Fig. 2(a), as the thickness of the shell surrounding the voids increases, the region within the shells begins to resemble a system of overlapping circles, which is the basis of their derivations. This is why the Philleo and the Pleau and Pigeon equations are more accurate at predicting larger percentiles of the paste-void spacing distribution.[12]

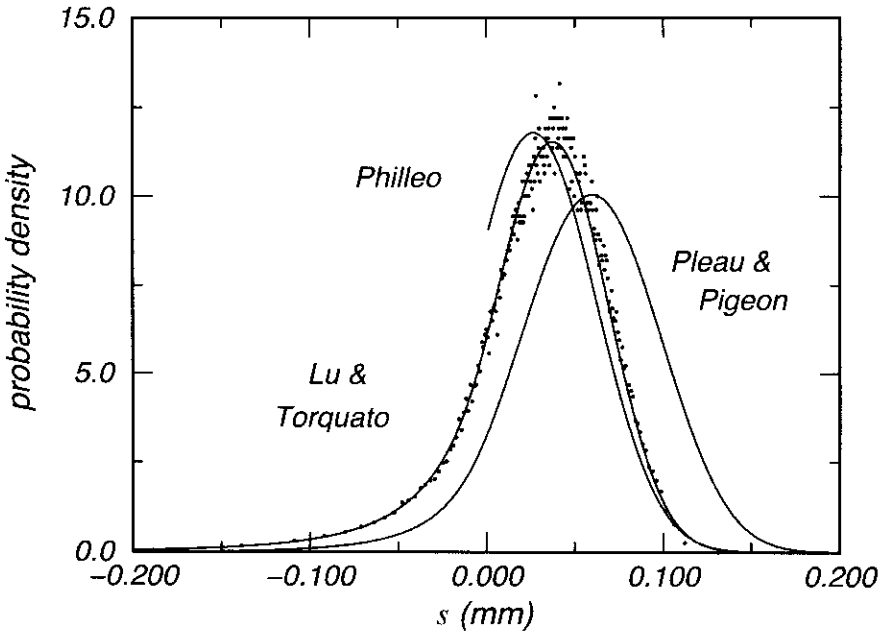

Figure 9. Estimates of the paste-void probability density function by Philleo, Pleau and Pigeon, and Lu and Torquato for lognormally distributed sphere radii with a number density of 240 mm^{-3}. Measured values are shown as filled circles. (From Ref. 12.)

Future Research

Given the recent interest in developing spacing equations, a number of issues should be resolved:

1. The results presented here assume that there exists sufficient inter-aggregate space to contain a statistical representation of the bulk air void system. This assumption should be tested for various aggregate volume fractions. For large aggregate fractions, one could expect that an insufficient number of voids exist within the inter-aggregate spaces, and that the critical void spacing should be smaller.
2. If the approximation of the air void radii by a lognormal distribution is valid, the parameters to the distribution could be used to convert the Powers spacing factor to an estimate of the 95th percentile of the paste-void spacing distribution.

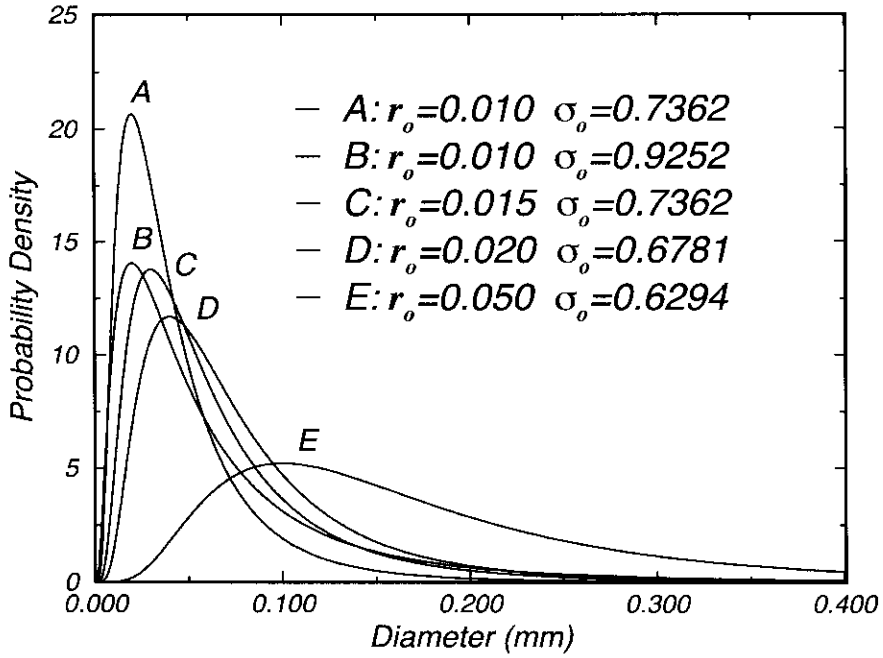

Figure 10. Air void diameter distributions used in the analytical test.

Protected Paste Volume

The concept of a "protected paste volume" (PPV) originated from Powers[3] and was extended by Larson et al.,[58] Fagerlund,[9] Philleo,[8] and Natesaiyer et al.[59,60] The concept assumes that each air void in concrete protects the spherical volume of paste that surrounds it from frost damage. Powers[3,88] called this zone the "sphere of influence" (SoI) of the air voids. The protected paste volume is then simply defined as the common volume of paste protected from frost damage by all the air voids present in the concrete. The ratio of the PPV to the total volume of air and paste is referred to as the protected paste ratio (PPR).[59]

Though the definition is simple, a researcher attempting to calculate the value for a given concrete is faced with an immediate decision: Is the zone of influence dependent on the material properties of the concrete, the freezing environment, and the size of the air void? Or is the zone of influence dependent only on the size of the air voids? The calculations are very sim-

ple if it is assumed that the thickness of the zone of influence is some constant value.[8,58] The calculations are more difficult if the zone of influence depends on the material properties of the concrete and the freezing environment as well.[59,60] However, if the material properties of concrete and the freezing environment are not considered, the calculations are simply an exercise in geometry and probability, and are valid for any material filled with spherical voids.

From the discussions in the previous sections, it might seem that the paste-void proximity spacing distribution might provide a way out of the difficulty. However, some reflection will show that the paste-void spacing distribution provides only a way to estimate what fraction of the cement paste is within some distance of an air void. They do not provide any guidance on what the critical distance should be for frost-resistant concrete. Of the proposed physical mechanisms of frost damage to concrete, currently only the hydraulic pressure theory has been developed sufficiently to provide estimates of the critical distance based on the material properties of the concrete and some measure of the freezing environment, and so it will be used for demonstration purposes.

Background

The first applications of the protected paste volume concept applied to air voids in concrete were performed by Warris[33,89] and by Larson, Cady, and Malloy.[58] They started with a parametric estimate of the chord distribution, and combined that with the Philleo spacing equation[8] to estimate the fraction of paste within some distance of an air void. The application was purely geometrical.

The concept was advanced by Natesaiyer et al.[59,60] by using the Powers hydraulic pressure theory.[3] The thickness of protected paste surrounding an air void is a function of the void radius. The volume of paste within any given shell would be the protected paste volume. However, this approach suffers from a number of drawbacks: Having a shell thickness that is a function of air void radius makes deriving analytic expressions for the protected paste volume difficult. The approach also depends upon a particular theory for freeze-thaw degradation.

The original protected paste volume concept of Larson, Cady, and Malloy has a number of advantages. For an arbitrary distribution of air void radii, numerically exact equations exist to calculate the fraction of paste within a given distance from each air void. The approach is independent of particular freeze-thaw degradation models. Either better materials science

Table IV. Values of $Q_{\bar{L}}$ for the Powers spacing equation*

r_0 (mm)	σ_0	α (mm^{-1})	Air content 0.06	0.09	0.12	0.15	0.18	0.21
0.100	0.0000	30	1.028	1.060	1.093	1.128	1.165	1.113
0.050	0.6294	15	1.360	1.370	1.386	1.406	1.430	1.349
0.020	0.6781	30	1.428	1.434	1.446	1.464	1.485	1.397
0.010	0.7362	45	1.522	1.522	1.530	1.544	1.562	1.465
0.015	0.7362	30	1.522	1.522	1.530	1.544	1.562	1.465
0.010	0.9252	15	1.965	1.941	1.928	1.925	1.927	1.791

*From Ref. 13.

Table V. Values of Q_F for the Philleo spacing equation*

r_0 (mm)	σ_0	α (mm^{-1})	Air content 0.06	0.09	0.12	0.15	0.18	0.21
0.100	0.0000	30	1.076	1.115	1.155	1.196	1.240	1.285
0.050	0.6294	15	0.958	0.970	0.985	1.004	1.024	1.048
0.020	0.6781	30	0.944	0.952	0.965	0.980	0.998	1.018
0.010	0.7362	45	0.926	0.931	0.940	0.952	0.967	0.984
0.015	0.7362	30	0.926	0.931	0.940	0.952	0.967	0.984
0.010	0.9252	15	0.874	0.867	0.865	0.867	0.872	0.878

*From Ref. 13.

Table VI. Values of Q_K for the Pleau and Pigeon spacing equation*

r_0 (mm)	σ_0	α (mm^{-1})	Air content 0.06	0.09	0.12	0.15	0.18	0.21
0.100	0.0000	30	1.074	1.108	1.140	1.169	1.196	1.221
0.050	0.6294	15	1.080	1.098	1.111	1.123	1.134	1.146
0.020	0.6781	30	1.072	1.085	1.096	1.106	1.115	1.125
0.010	0.7362	45	1.061	1.070	1.077	1.084	1.091	1.099
0.015	0.7362	30	1.061	1.070	1.077	1.084	1.091	1.099
0.010	0.9252	15	1.022	1.020	1.017	1.016	1.016	1.018

*From Ref. 13.

or simply laboratory tests could be used to establish both the fraction of paste that must be protected and the distance this fraction needs to be within an air void surface.

Constant Shell Thickness

As a first approximation, one could begin by assuming that, for some physical model of freeze-thaw, the SoI radius is a constant for all air void radii. Once this thickness is determined from the cement paste properties and the freezing rate, the calculation would then be identical to determining the paste-void spacing distribution as was done in the previous section.

While it would seem that a constant SoI radius is unlikely, this approach has a number of advantages. This approach can be developed independently of a freeze-thaw mechanism. In fact, the critical Powers spacing factor derived by Powers was based upon the hydraulic pressure theory, which has since been shown to have serious flaws. Yet it has been shown by Pigeon and coworkers that there exist critical values of $\bar{L}$ depend on the material properties of the concrete and the exposure conditions.

Variable Shell Thickness

A more rigorous approach is to calculate the protected paste thickness as a function of the void radius. Figure 11 depicts the idea schematically. Borrowing from the notation of Powers,[3] an air void with radius r_b protects a shell of paste out to a radius r_m from the center of the void. The shell thickness s is the difference $s = r_m - r_b$.

An estimate of the volume of paste protected was derived by Natesaiyer et al.[59] They approximated the system of r_m radius spheres by overlapping spheres. The protected paste ratio Ω follows from the Hertz[64] distribution:

$$\Omega = 1 - \exp\left[\frac{-4\pi\, n}{3}\left\langle R_m^3\right\rangle\right] \tag{123}$$

The performance of the Philleo and the Pleau and Pigeon spacing equations discussed in the previous section suggests that the approximation may be sufficiently accurate as the value of Ω approaches 1.

The air content of the paste A_p was used to simplify the equation[59]:

$$\Omega = 1 - \exp\left[-A_p \frac{\left\langle R_m^3\right\rangle}{\left\langle R_b^3\right\rangle}\right] \tag{124}$$

Certain limiting cases demonstrate similarities to spacing equations. In the limit $\langle R_b^3 \rangle \rightarrow 0$, the voids have zero radius and $r_m = s$:

$$\Omega|_{\langle R_b^3 \rangle \rightarrow 0} = 1 - \exp\left[\frac{-4\pi n}{3} s^3\right] \tag{125}$$

This equation bears a resemblance to the Philleo approach. Conversely, in the limit that s is a constant, the quantity $\langle R_m^3 \rangle$ can be expanded in terms of $\langle R_b^3 \rangle$ and s:

$$\Omega|_{r_m = s + r_b} = 1 - \exp\left[-A_P \left(1 + \alpha s + \alpha \frac{\langle R_b \rangle}{\langle R_b^2 \rangle} s^2 + \frac{\alpha}{3\langle R_b^2 \rangle} s^3\right)\right] \tag{126}$$

This result is directly related to that of Fagerlund.[9] The overall approach has the drawback that for $s \rightarrow 0$, the PPR Ω equals the volume of the corresponding system with overlapping spheres; this was the same deficiency as for the Pleau and Pigeon equation.

Freeze-Thaw Model

The development thus far for the variable SoI thickness has been done without regard to a specific model for freeze-thaw. Fundamentally, all one needs in order to proceed further is an analytical relationship between r_m and r_b. As an example, consider the Powers hydraulic pressure theory used in Natesaiyer et al.[59] The model requires a number of material and environmental quantities:

- k: cement paste permeability coefficient
- T: cement paste tensile strength
- μ: pore fluid viscosity
- S: capillary pore saturation
- u: volume of water frozen per volume paste, per degree
- θ: cooling rate

The radius r_m can be expressed as a function of the air void radius r_b and material properties of the concrete[3]:

$$\frac{r_m^3}{r_b} + \frac{r_b^2}{2} - \frac{3}{2} r_m^2 = \frac{3\,k\,T}{\mu\left(1.09 - S^{-1}\right) u\,\theta} \tag{127}$$

The left side of the equation is purely geometric, and the right side is purely material. For brevity, the materials term can be represented by Φ, and the material dependence is implied. Also, the geometric portion of the equation can be simplified slightly by expressing the result as a function of the shell thickness $s = r_m - r_b$ [3]:

$$\frac{s^3}{r_b} + \frac{3\,s^2}{2} = \Phi \tag{128}$$

The shell thickness s for a material parameter $\Phi = 0.1$ mm^2 is shown in Fig. 12(a). Assuming a capillary porosity $\varepsilon = 0.08$, the ratio of expelled volume of water to the volume of void is shown in Fig. 12(b). This ratio cannot be greater than unity. Using this physical limit, the corrected shell thickness in Fig. 12(a) is shown as a dashed line.

Once the functional relationship between the SoI radius r_m and the void radius r_b is established, the protected paste ratio Ω can be calculated using Eq. 124 above. Consider a concrete with a paste material parameter $\Phi = 0.1$ mm^2 and a porosity $\varepsilon = 0.08$. Using the five air void radius distributions shown in Fig. 10, the protected paste ratio Ω, calculated as a function of air content within the paste A_p, is shown in Fig. 13(a).

Similarly, the Powers spacing factor $\overline{L}$ can also be calculated for these systems as a function of paste air content A_p. Figure 13(b) shows a plot of Ω versus $\overline{L}$ for the five radius distributions. For these particular values of Φ and ε, the relationship between Ω and $\overline{L}$ seems to be relatively insensitive to the air void radius distribution. All the distributions but one appear to have a critical value of $\overline{L}$ near 0.300 μm for these values of Φ and ε. This result could help explain the success of the critical spacing factor approach to characterizing concrete performance to freezing and thawing.[90]

Future Research

New and more sophisticated freeze-thaw models are being developed. If air voids are the key to ideal performance under conditions of freezing and thawing, sufficiently sophisticated theories are needed to determine the quantity and "quality" of the air void distribution required for optimum performance.

1. It is reasonable to assume that other models for freeze-thaw will also show that the hydraulic pressures are relieved at the air voids. Therefore, the corresponding equations that relate geometry to material properties will resemble Eq. 128. It would be useful to

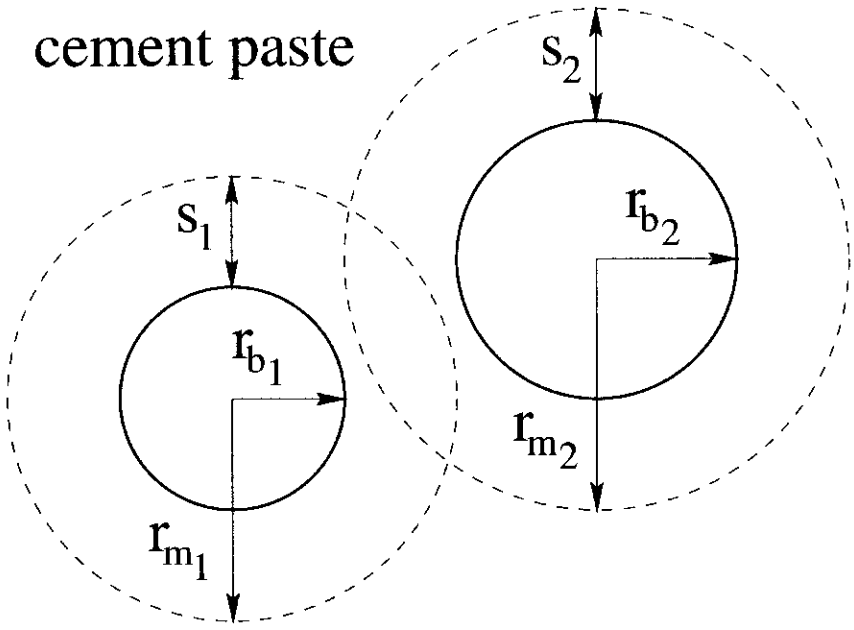

Figure 11. Sphere of influence for two air voids (r_{b1},r_{b2}) in proximity to one another. The radii of the protected paste zones are r_{m1} and r_{m2}, respectively.

generalize a pressure relief theory in order to obtain a generalized form for Eq. 128. Success in this endeavor would demonstrate why the Powers spacing factor has performed so well for so long.

2. The estimate of the protected paste ratio shown here is based upon a simple, overlapping sphere model. It would be useful to extend the Lu and Torquato equation to include varying shell thicknesses in order to develop a more accurate microstructural model.

Summary

This chapter is an introduction to the complete characterization of the air void system in hardened concrete. This characterization includes information regarding volumetric data and an ASTM C 457 analysis, the air void size distribution, and the paste-air system microstructure.

The present test methods in ASTM C 457 have been useful tools for the concrete industry. However, as use of performance requirements increases, the matter of performance acceptance will have to address uncertainty in

test results. Further, rational performance acceptance criteria can be formulated only with an understanding of the probable uncertainties in the test method results. For this reason, a detailed discussion of uncertainty in the ASTM C 457 method has been addressed.

Although tabulating individual chord lengths is not currently required by the existing ASTM C 457 test method, it may become a future requirement. This information could be used to extract information regarding the air void diameter distribution. At the very least, this information would be a useful research tool. Given the ubiquitous presence of computers and computerized automation, the tabulation of the individual chord lengths by computer would not add to the work load of the petrographer, but would contribute substantially to the characterization of the air void distribution.

The last piece of the freeze-thaw puzzle is the paste-air microstructure. There are two parts to freeze-thaw performance in concrete: the mechanism of freezing and the pressures generated, and the mechanism of pressure release by the air voids. The mechanism of freezing and pressure generation is a materials science problem. The effectiveness of the air voids, due to their proximity to either the paste or to one another, is purely a stereology problem. Accurate prediction of freeze-thaw performance requires an understanding of both parts, which are brought together in the formulation of the protected paste ratio.

The compilation and distillation of available knowledge within a particular field of study serves two purposes. Expressing what is known delineates the problems that are currently solvable. At the same time, it delineates where additional work is needed to either verify existing assumptions or to advance understanding. Some of the remaining problems in characterizing air voids have been enumerated in the previous sections, so that this chapter serves not only as a primer on air void characterization, but also as a starting point for future research.

Appendix A: Uncertainty

The definitions for expressing uncertainty in measurements have been standardized by ISO.[91] These definitions have been summarized in a shorter document published by the National Institute of Standards and Technology.[92] There are a number of good books that address uncertainty analysis. Classic texts include Mandel[93] and Wilson.[94] The books by Taylor[95] and Dieck[96] are ISO compliant.

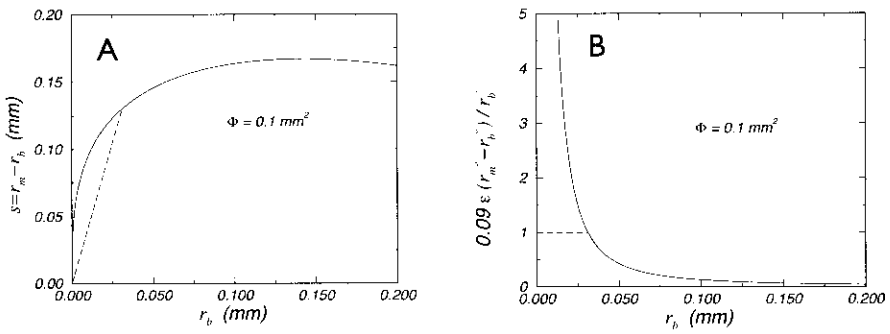

Figure 12. The shell thickness s (a) and the ratio of expelled ice volume to the volume of the air void (b). The solid line is the original equation by Powers, the dashed line accounts for the finite volume of the air void. (From Ref. 59. Used with permission.)

Let there be a physical process from which values of X are measured. The individual values X_i differ from the true x by the random error ε_i:

$$X_i = x + \varepsilon_i \tag{129}$$

Fundamentally, the error ε_i is unknowable. Repeated measurements will yield a distribution of X_i values. The dispersion in these values is represented by the standard uncertainty $u(x)$. The particular functional form for $u(x)$ depends upon the distribution of the errors ε_i. In principle, the experimenter chooses an appropriate distribution function. Here, all errors will be characterized by a normal distribution with mean zero and variance σ_X^2. Therefore, σ_X represents the standard uncertainty in determining x.

For most uncertainty analyses, the final quantity of interest is calculated from a number of measured quantities. The uncertainty in the final quantity is the combined standard uncertainty u_c. One of the most lucid derivations for u_c, based upon a Taylor expansion, is given in the ISO document.[91] What follows is taken nearly verbatim from this document:

Let the response y depend upon N variables, each labeled x_i. Assuming that $\langle Y \rangle = f(\langle X_1 \rangle, \langle X_2 \rangle, \ldots, \langle X_N \rangle)$, the response y can be expanded about the expected value $\langle Y \rangle$ for a single experiment:

$$y - \langle Y \rangle = \sum_{n=1}^{N} \frac{\partial f}{\partial x_n} \left(x_n - \langle X_n \rangle \right) \tag{130}$$

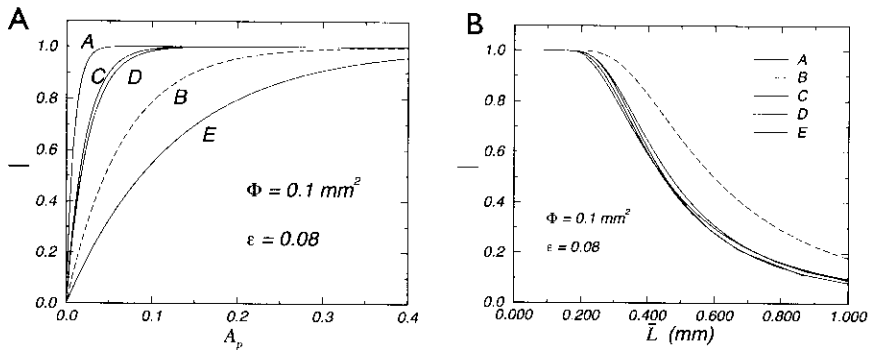

Figure 13. The protected paste ratio Ω as a function of paste air content A_p (a) and Powers spacing factor $\bar{L}$ (b). The air void radius distributions are the same as those shown in Fig. 10.

The square of this deviation can be expressed succinctly:

$$\left(y-\langle Y\rangle\right)^2=\sum_{n=1}^{N}\left(\frac{\partial f}{\partial x_n}\right)^2\left(x_n-\langle X_n\rangle\right)^2 +2\sum\sum\frac{\partial f}{\partial x_n}\frac{\partial f}{\partial x_m}\left(x_n-\langle X_n\rangle\right)\left(x_m-\langle X_m\rangle\right) \tag{131}$$

One next takes the expectation of both sides. The result is simplified because of the Gaussian error model. The expectation of the left side is simply the variance in y:

$$\sigma_y^2=\sum_{n=1}^{N}\left(\frac{\partial f}{\partial x_n}\right)^2\sigma_n^2+2\sum_{n=1}^{N-1}\sum_{m=n+1}^{N}\frac{\partial f}{\partial x_n}\frac{\partial f}{\partial x_m}\sigma_{nm} \tag{132}$$

The quantity σ_n^2 replaces $\langle(x_n-\langle X_n\rangle)^2\rangle$. The quantity σ_{nm} is the covariance between x_n and x_m and is shorthand for $\langle(x_n-\langle X_n\rangle)(x_m-\langle X_m\rangle)\rangle$. In summary, the combined standard uncertainty is the standard deviation in y. Note that σ_y does not use the random variable notation to distinguish it from a standard uncertainty. The corresponding estimated standard deviation in y is expressed as s_y.

Coefficient of Variation

The coefficient of variation η is the ratio of the standard deviation to the expected value:

$$\eta_X = \frac{\sigma_X}{\langle X \rangle} \tag{133}$$

The corresponding quantity based upon measured values is denoted C_X, and is the ratio of the estimated standard deviation s_X to the average value $\overline{X}$:

$$C_X = \frac{s_X}{\overline{X}} \tag{134}$$

Many of the equations considered in the subsequent sections are multiplicative. For example, consider a calculated quantity z that is a simple function of the random variables X and Y: $z = XY$. The estimated combined standard uncertainty in z, assuming no covariance in X and Y, is calculated from Eq. 132:

$$\begin{aligned} s_z^2 &= \left(\frac{\partial z}{\partial X}\right)^2 s_X^2 + \left(\frac{\partial z}{\partial Y}\right)^2 s_Y^2 \\ &= Y^2 s_X^2 + X^2 s_Y^2 \end{aligned} \tag{135}$$

Since $\bar{z} = \overline{XY}$, the above expression be expressed compactly using the coefficient of variation C_z:

$$C_z^2 = C_X^2 + C_Y^2 \tag{136}$$

Appendix B: Probability and Statistics

The topics discussed in this chapter rely upon the concepts of random variables, probability theory, and statistics. It will be useful to discuss these topics in detail to ensure uniformity throughout the sections. A number of excellent books exist for additional information and discussion.[97,98]

Random Variables

A useful way to introduce the idea of random variables is through an example. Consider an experiment that has inherent randomness. The result of the experiment is a single value, out of a number of possible values. The result of a single experiment may be represented by the random variable X. The possible values that X may take can be represented by the variable x. For an experiment consisting of a coin toss, the possible outcomes are either heads H or tails T. The variable x can represent the set of outcomes, $x = \{H,T\}$. The random variable X may take on the value of either H or T. From experience, one knows that the probability P of either event is one-half:

$$P(X=H) = P(X=T) = \frac{1}{2} \tag{137}$$

Probability Density Function

In contrast to the coin toss experiment, consider an experiment where X can be any real number on the interval [0,1]. In this case, there are an infinite number of possible values X can take, and X is a continuous random variable. Since the number of possible outcomes is infinite, the probability that $X = 0.5$ is zero. For a continuous random variable, one can only define a probability density function $f(x)$ such that

$$P(a \le X \le b) = \int_a^b f(x)\,dx \tag{138}$$

under the constraints

$$\int_{-\infty}^{+\infty} f(x)\,dx = 1 \qquad f(x) \ge 0 \tag{139}$$

This definition is consistent with the fact that the probability of a particular outcome such as $X = a$ is zero:

$$P(a \le X \le a) = \int_a^a f(x)\,dx = 0 \tag{140}$$

Cumulative Distribution Function

When analyzing measured data, it is often more convenient to work with the cumulative distribution function (CDF), also referred to as the probability function. For a probability density function $f(x)$, the cumulative distribution function $F(x)$ is the probability that a particular outcome can be less than x:

$$F(x) = P(x \leq X) \tag{141}$$

For a continuous probability density $f(x)$, the quantity has the following mathematical definition:

$$F(x) = \int_{-\infty}^{x} f(x')\, dx' \tag{142}$$

Point Probability Function

When the possible outcomes are either finite or countably infinite (e.g., all positive prime numbers), the discrete random variable X is characterized by a point probability function $p(x)$:

$$P(X = a) = p(a) \tag{143}$$

Here, the point probability function will be treated as a special case of the continuous probability density function. While investigating air void radius distributions, it may be useful at times to consider the monosized sphere radius distribution having radius r_0:

$$P(R{=}r_0) = p(r_0) = 1 \tag{144}$$

However, the subsequent sections will summarize equations for continuous random variables. As a solution, one can represent the monosized probability density function $f(x)$ by a Dirac delta function $\delta(x)$ (see Appendix C). For a system of monosized sphere radii, the PDF $f(r)$ can be expressed as a delta function:

$$f(r) = \delta(r - r_0) \tag{145}$$

Mixtures of monosized sphere radii, each denoted by radius r_i, are composed of weighted delta functions

$$f(r) = \sum_i \gamma_i \, \delta(r - r_i) \tag{146}$$

such that $\gamma_i = 1$. The coefficients γ_i represent the number fraction of radius r_i.

Statistics

Under many circumstances one can sufficiently characterize the air void radius distribution in concrete from certain statistical properties, and the functional form for the radius probability density function is not required.

Expected Values

Let the random variable X take values from the continuous probability density function $f(x)$. The expectation of X has the following definition:

$$\langle X \rangle = \int_{-\infty}^{+\infty} x \, f(x) \, dx \tag{147}$$

with the following constraint:

$$\int_{-\infty}^{+\infty} |x| \, f(x) \, dx < \infty \tag{148}$$

Similarly for higher powers of X:

$$\langle X^n \rangle = \int_{-\infty}^{+\infty} x^n \, f(x) \, dx \tag{149}$$

Let $f(r)$ represent the air void radius probability density function. Quantities like the expected average surface area S and the expected volume V can be expressed as expectations of the radius distribution:

$$\begin{aligned} S &= 4\pi \langle R^2 \rangle \\ V &= \frac{4\pi}{3} \langle R^3 \rangle \end{aligned} \tag{150}$$

Averages

The preceding section is distinguished from averages. Expectations are calculated from equations. Averages are calculated from measured data. Consider an experiment with random variables X_i from N trials. The average value $\overline{X}$ is

$$\overline{X} = \frac{1}{N}\sum_{i=1}^{N} X_i \tag{151}$$

Similarly for higher powers of X_i:

$$\overline{X^n} = \frac{1}{N}\sum_{i=1}^{N} X_i^n \tag{152}$$

An experiment is conducted with the assumption that $\overline{X^n}$ is an unbiased estimator of $\langle X^n \rangle$.

Variance

The variation in a population of random variables X_i are typically expressed as a standard deviation σ_X. However, it is the variance σ_X^2 that more easily expressed mathematically:

$$\begin{aligned}\sigma_X^2 &= \left\langle \left(x - \langle X \rangle\right)^2 \right\rangle \\ &= \langle X^2 \rangle - \langle X \rangle^2\end{aligned} \tag{153}$$

The kth moment is defined as $\langle (x - \langle X \rangle)^k \rangle$.[97] Therefore, the variance is the second moment about the mean $\langle X \rangle$. However, it is common for publications to use the term "moment" to mean expectation. In that context, the term is correct if one is calculating the moment about zero mean.

Appendix C: Delta Function Distribution

The Dirac delta function $\delta(x)$ is a useful tool for representing discrete probability distributions as continuous distributions. A useful discussion of the Dirac delta function can be found either in Lighthill[99] or in any suitable

mathematical physics text such as Arfken.[68] For purposes of this chapter, the Dirac delta function can be thought of as a Gaussian in the limit that the variance approaches zero.

The Dirac delta function can be described rigorously using a few definitions. The function itself has the following nondifferentiable characteristic:

$$\delta(x - x_0) = \begin{cases} \infty & x = x_0 \\ 0 & otherwise \end{cases} \tag{154}$$

However, the area under the Dirac delta function is unity:

$$\int_{-\infty}^{+\infty} \delta(x)\, dx = 1 \tag{155}$$

The function also has the following convolution property for an arbitrary function $f(x)$:

$$\int_a^b \delta(x - x_0)\, f(x)\, dx = \begin{cases} f(x_0) & a \le x_0 \le b \\ 0 & otherwise \end{cases} \tag{156}$$

A point probability distribution can be replaced by a Dirac delta function. Given a point probability function $p(x)$ that describes the outcomes of a random trial, let $p(x_0)$ represent the probability that the random variable X equals x_0. The corresponding continuous function representation would be $p(x_0)\delta(x - x_0)$.

Monosized Spheres

The same applies to monosized sphere radius distributions. A distribution of monosized radius r_0 can be represented by $f(r) = \delta(r - r_0)$. The nth moment can be calculated directly:

$$\begin{aligned} \langle R^n \rangle &= \int_0^\infty r^n\, \delta(r - r_0)\, dr \\ &= r_0^n \end{aligned} \tag{157}$$

This demonstrates the greatest usefulness of the Dirac delta function as a representation of a monosized void system. Using the delta function, one can then use the tools developed for continuous functions.

Point Probability

The Dirac delta function is also useful for describing a distribution composed of a finite number of sphere radii. This would be useful for approximating data from a sieve analysis. Let $f(r)$ represent the combined sphere radius distribution. Let γ_i represent the probability that there exists a sphere with radius R_i. Let there be N such possible radii. The PDF $f(r)$ can be expressed as a linear sum of each radius:

$$f(r) = \sum_{i=1}^{N} \gamma_i \, \delta(r - R_i) \tag{158}$$

The values of γ_i are constrained to sum to one:

$$\sum_{i=1}^{N} \gamma_i = 1 \tag{159}$$

Circle Distribution

Consider a monosized sphere diameter distribution $f(x)$, with every sphere of diameter x_0. The corresponding circle diameter distribution $g(y)$ is calculated from Eq. 41:

$$\begin{aligned} g(y) &= \frac{y}{\langle X \rangle} \int_y^\infty \frac{\delta(x - x_0)}{\left(x^2 - y^2\right)^{1/2}} \, dx \\ &= \frac{y}{x_0} \frac{1}{\left(x_0^2 - y^2\right)^{1/2}} \qquad y \le x_0 \end{aligned} \tag{160}$$

Chord Distribution

The corresponding chord distribution $h(z)$ can be calculated from Eq. 49:

$$\begin{aligned} h(z) &= \frac{2z}{\langle X^2 \rangle} \int_z^\infty \delta \, (x - x_0) \, dx \\ &= \frac{2z}{x_0^2} \qquad z \le x_0 \end{aligned} \tag{161}$$

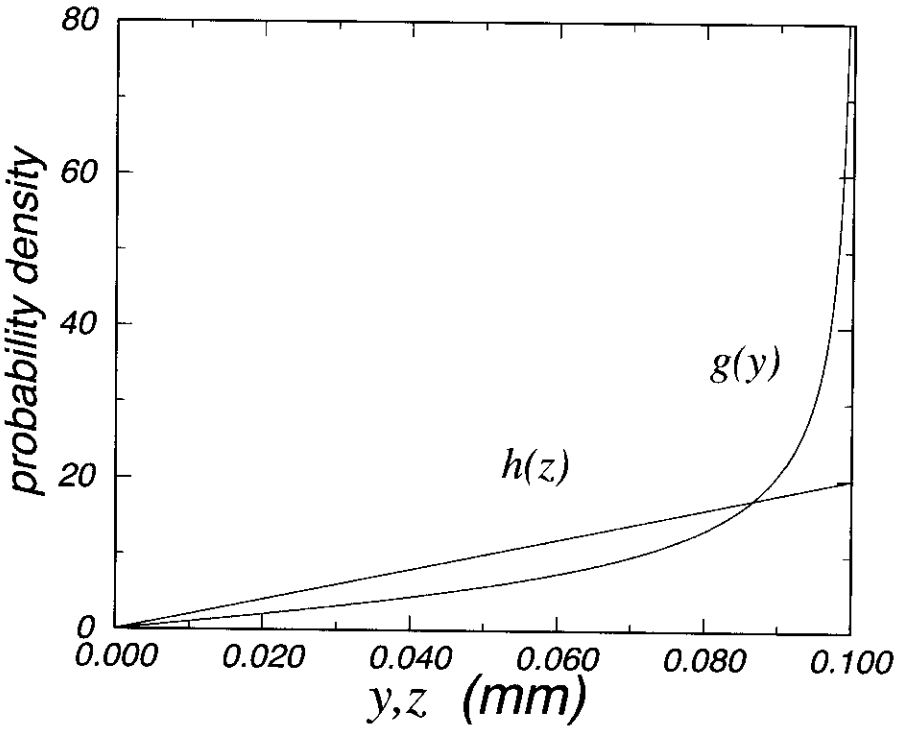

Figure 14. The circle diameter distribution $g(y)$ and the chord distribution $h(z)$ for a monosized 0.100 mm sphere diameter distribution.

Example

The circle diameter distribution $g(y)$ and the chord distribution $h(z)$ for a monosized 100 μm diameter sphere are shown in Fig. 14. The corresponding sphere diameter distribution would appear as a vertical line at 0.100 mm. The shape of $g(y)$ suggests that there is a propensity for intersecting spheres near their equators. The function $h(z)$ in the figure shows the contribution to the chord distribution from a particular sphere size. The sum total of a number of a finite number of different monosized spheres would be the sum total of the corresponding $h(z)$. It is this property that was exploited by Lord and Willis.[50]

Appendix D: Lognormal Distribution

A thorough discussion of the logarithmic family of distributions can be found in Ref. 87. The general nth order logarithmic distribution has the following form[87]:

$$f_n(x) = \frac{x^n \exp\left[-\frac{1}{2}\left(\frac{\ln x - \ln x_n}{\sigma_n}\right)^2\right]}{\sqrt{2\pi}\,\sigma_n\, x_n^{n+1} \exp\left[(n+1)^2\,\sigma_n^2/2\right]} \tag{162}$$

The expectations can also be expressed in a generalized form:

$$\left\langle X^k \right\rangle_n = x_n^k \exp\left[\left(k^2 + 2k + 2kn\right)\sigma_n^2/2\right] \tag{163}$$

The function $f_n(x)$ is the same for all values of n. Only the meaning of x_n varies. There are three values of n that are typically of interest to experimenters:

$x_{-3/2}$: mean
x_{-1}: median
x_0: mode

The parameters can be mapped onto one another. Compare the ratio of the first moment to the second moment for an nth order and an mth order distribution:

$$\frac{x_n\, e^{(2n+3)\sigma_n^2/2}}{x_m\, e^{(2m+3)\sigma_n^2/2}} = \frac{x_n^2\, e^{(4n+8)\sigma_n^2/2}}{x_m^2\, e^{(4m+8)\sigma_n^2/2}} \tag{164}$$

Solving this equation for σ demonstrates that the meaning of σ is identical for all n and m:

$$\sigma_m = \sigma_n = \sigma \tag{165}$$

Given this, the parameters x_n and x_m can be mapped to one another:

$$\frac{x_n}{x_m} = e^{(m-n)\sigma^2} \tag{166}$$

Specific Surface

From the material presented so far, the specific surface can be calculated directly. Let $f_n(x)$ represent a sphere diameter distribution. The specific surface is the ratio of two moments:

$$\alpha = 6\frac{\langle X^2 \rangle}{\langle X^3 \rangle} = \frac{6}{x_n}\exp\left[-(2n+7)\,\sigma_n^2/2\right] \tag{167}$$

Chord Distribution

The corresponding chord length distribution can be calculated from Eq. 49:

$$h(z) = \frac{2z}{\langle X^2 \rangle}\int_z^\infty f_n(x)\,dx = \frac{z}{\langle X^2 \rangle}\,erfc\left(\frac{\ln z - \ln x_n}{\sqrt{2}\,\sigma_n} - \frac{(n+1)}{\sqrt{2}}\,\sigma_n\right) \tag{168}$$

The function $erfc(x)$ is the complementary error function.[67] For parametric studies using lognormally distributed sphere diameters, the moments of the chord distribution are quite useful:

$$\langle Z^k \rangle_n = \frac{2}{k+2}\frac{\langle X^{k+2} \rangle}{\langle X^2 \rangle} = \frac{2\,x_n^k}{k+2}\exp\left[\left(k^2 + 6k + 2nk\right)\sigma_n^2/2\right] \tag{169}$$

Example

The circle diameter distribution $g(y)$ and the chord length distribution $h(z)$ for a zeroth-order logarithmic sphere diameter distribution $f(x)$ are shown in Fig. 15. As the dimensionality of the probe decreases (spheres–circles–chords), the corresponding distribution widens due to the cumulative contribution of larger sphere diameters. This is true for the logarithmic distribution, but can be far different for other distributions. In fact, some distributions are invariant: $f(x) = g(y) = h(z)$.

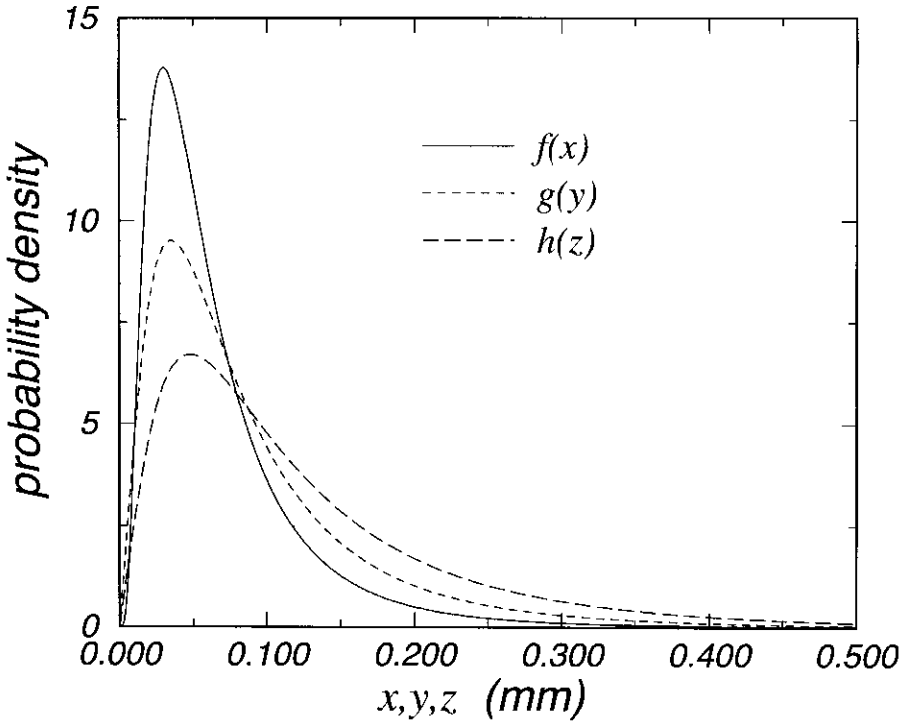

Figure 15. The circle diameter distribution $g(y)$ and the chord length distribution $h(z)$ for a zeroth-order logarithmic sphere diameter distribution $f(x)$ with modal diameter 0.030 mm and $\sigma_0 = 0.7362$.

References

1. ASTM C457: Standard test method for microscopical determination of parameters of the air-void system in hardened concrete. American Society for Testing and Materials, West Conshohocken, Pennsylvania, 1990.
2. K.C. Hover, "Air content and unit weight of hardened concrete"; p. 296 in *Significance of Tests and Properties of Concrete and Concrete-Making Materials,* STP 169C. Edited by Lamond and Kleiger. American Society for Testing and Materials, Philadelphia, 1994.
3. T.C. Powers, "The air requirement of frost-resistant concrete," *Proc. Highway Res. Board,* **29**, 184, (1949).
4. A. Rosiwal, "Über geometrische gesteinsanalysen. ein einfacher weg zur ziffermässigen feststellung des quantitätsverhältnisses der mineralbestandtheile gemengter gesteine," *Verhandl. der K.-K. geologischen Reichsanstalt,* 5/6, 143 (1898).
5. L.S. Brown and C.U. Pierson, "Linear traverse technique for measurement of air in hardened concrete," *J. ACI,* **22**, 117 (1950).

6. S.D. Wicksell, "The corpuscle problem: A mathematical study of a biometric problem," *Biometrika,* **17**, 84 (1925).
7. W.P. Reid, "Distribution of sizes of spheres in a solid from a study of slices of the solid," *J. Math. Phys.,* **34**, 95 (1955).
8. R.E. Philleo, "A method for analyzing void distribution in air-entrained concrete," *Cem. Concr. Aggregates,* **5**, 128 (1983).
9. G. Fagerlund, "Equations for calculating the mean free distance between aggregate particles or air-pores in concrete," *CBI Forskning/Research,* **8**, 77 (1977).
10. R. Pleau and M. Pigeon, "The use of the flow length concept to assess the efficiency of air entrainment with regards to frost durability: Part I — Description of the test method," *Cem. Concr. Aggregates,* **18**, 19 (1996).
11. E.K. Attiogbe, "Mean spacing of air voids in hardened concrete," *ACI Mater. J.,* **90**, 174 (1993).
12. K.A. Snyder, "A numerical test of air void spacing equations," *Adv. Cem. Based Mater.,* **8**, 28 (1998).
13. K.A. Snyder, "Estimating the 95th percentile of the paste-void proximity distribution"; to be published in *RILEM Workshop on Freeze-Thaw Performance of High Performance Concrete.* Edited by D. Janssen and M. Snyder. Minneapolis, Minnesota, 1999.
14. E.E. Underwood, *Quantitative Stereology.* Addison-Wesley, Reading, Massachusetts, 1970.
15. G.J. Verbeck, "The camera lucida method for measuring air voids in hardened concrete," *J. ACI,* **18**, 1025 (1947).
16. A. Delesse, "Pour déterminer la composition des roches," *Ann. des Mines,* **13**, 379 (1848).
17. J.E. Hilliard, "Volume fraction analysis by quantitative metallography," Technical report, General Electric Research Laboratory, March 1961.
18. F. Chayes, *Petrographic Modal Analysis.* John Wiley, New York, 1956.
19. S.A. Saltykov, *Stereometric Metallography,* 2nd ed. Metallurgizdat, Moscow, 1958.
20. E.R. Weibel, *Morphometry of the Human Lung.* Springer-Verlag, Berlin, 1963.
21. D. McLean, *Grain Boundaries in Metals.* Oxford University Press, London, 1957.
22. S.A. Saltykov, "A stereological method for measuring the specific surface area of metallic powders"; p. 63 in *Stereology.* Edited by H. Elias. Springer-Verlag, 1967.
23. S.I. Tomkeieff, "Linear intercepts, areas and volumes," *Nature,* **155**, 24 (1945).
24. H.W. Chalkley, J. Cornfield, and H. Park, "A method for estimating volume-surface ratios," *Science,* **110**, 295 (1949).
25. T.F. Willis, "Measuring air in hardened concrete," *Proc. Am. Concr. Inst.,* **48**, 901 (1952).
26. K. Mather, "Measuring air in hardened concrete," *Proc. Am. Concr. Inst.,* **49**, 61 (1953).
27. H. Sommer, "The precision of the microscopical determination of the air-void system in hardened concrete," *Cem. Concr. Aggregates,* **1**, 49 (1979).
28. B.W. Langan and M.A. Ward, "Determination of the air-void system parameters in hardened concrete - an error analysis," *ACI J.,* **83**, 943 (1986).
29. R. Pleau and M. Pigeon, "Precision statement for ASTM C 457 practice for microscopical determination of air-void content and other parameters of the air-void system in hardened concrete," *Cem. Concr. Aggregates,* **14**, 118 (1992).

30. K. Snyder, K. Hover, and K. Natesaiyer, "An investigation of the minimum expected uncertainty in the linear traverse technique," *Cem. Concr. Aggregates,* **13**, 3 (1991).
31. J.E. Hilliard and J.W. Cahn, "An evaluation of procedures in quantitative metallography for volume fraction analysis," *Trans. Metal. Soc. AIME,* **221**, 344 (1961).
32. G.M. Tallis, "Estimating the distribution of spherical and elliptical bodies in conglomerates from plane sections," *Biometrics,* **26**, 87 (1970).
33. B. Warris, "The Influence of Air-Entrainment on the Frost Resistance of Concrete — Part A. Void Distribution"; in *Swedish Cement and Concrete Research Institute Proceedings NR 35.* Stockholm, 1963.
34. K.A. Snyder, K.C. Hover, K. Natesaiyer, and M. Simon, "Modeling air-void systems in hydrated cement paste," *Microcomp. Civ. Eng.,* **6**, 35 (1991).
35. K.C. Hover, "Analytical investigation of the influence of air bubble size on the determination of the air content of freshly mixed concrete," *Cem. Concr. Aggregates,* **10**, 29 (1988).
36. S.D. Wicksell, "The corpuscle problem: A case of ellipsoidal corpuscles," *Biometrika,* **18**, 152 (1926).
37. W.L. Nicholson, "Estimation of linear properties of particle size distributions," *Biometrika,* **57**, 273 (1970).
38. G.S. Watson, "Estimating functionals of particle size distributions," *Biometrika,* **58**, 483 (1971).
39. M.G. Kendall and P.A.P. Moran, *Geometrical Probability.* Hafner Publishing Co., New York, 1963.
40. E.B. Jensen, "A design-based proof of Wicksell's integral equation," *J. Microscopy,* **136**, 345 (1984).
41. J. Mecke and D. Stoyan, "Stereological problems for spherical particles," *Mathematische Nachrichten,* **96**, 311 (1980).
42. L.M. Cruze-Orive, "Distribution-free estimation of sphere size distribution from slabs showing overprojection and truncation, with a review of previous methods," *J. Microscopy,* **131**, 265 (1983).
43. E.T. Whittaker and G.N. Watson, *A Course in Modern Analysis,* 4th ed. Cambridge University Press, Cambridge, 1952.
44. R. Courant and D. Hilbert, *Methods of Mathematical Physics.* Wiley, 1989.
45. R.S. Anderssen and A.J. Jakeman, "Abel type integral equations in stereology — II. Computational methods of solution and the random spheres approximation," *J. Microscopy,* **105**, 135 (1975).
46. L.R. Roberts and P. Scheiner, "Microprocessor-based linear traverse apparatus for air-void distribution analysis"; p. 135 in *Proceedings of the Third International Conference on Cement Microscopy.* Edited by G.R. Gouda. International Cement Microscopy Association, 1981.
47. H. Elias, ed., *Stereology.* Springer-Verlag, 1967.
48. R.T. DeHoff and F.N. Rhines, eds., *Quantitative Microscopy.* McGraw-Hill, 1968.
49. R.L. Fullman, "Measurement of particle sizes in opaque bodies," *J. Metals,* **5**, 447 (1953).
50. G.W. Lord and T.F. Willis, "Calculation of air bubble size distribution from results of a Rosiwal traverse of aerated concrete," *ASTM Bull.,* **177**, 56 (1951).

51. T. Aarre, "Influence of measurement technique on the air-void structure of hardened concrete," *ACI Mater. J.*, **92**, 599 (1995).
52. R. Coleman, "The sizes of spheres from profiles in a thin slice, II. Transparent spheres," *Biometrical J.*, **25**, 745 (1983).
53. K. Snyder, "Discussion of 'Influence of measurement technique on the air-void structure of hardened concrete,' by T. Aare," *ACI Mater. J.*, **93**, 512 (1996).
54. B. Lu and S. Torquato, "Nearest-surface distribution functions for polydispersed particle systems," *Phys. Rev. A*, **45**, 5530 (1992).
55. B. Lu and S. Torquato, "Chord-length and free-path distribution functions for many-body systems," *J. Chem. Physics*, **98**, 6472 (1993).
56. R. Pleau, M. Pigeon, J.L. Laurencot, and R. Gagné, "The use of the flow length concept to assess the efficiency of air entrainment with regards to frost durability: Part II — Experimental results," *Cem. Concr. Aggregates*, **18**, 30 (1996).
57. E.K. Attiogbe, "Predicting freeze-thaw durability of concrete — A new approach," *ACI Mater. J.*, **93**, 457 (1996).
58. T.D. Larson, P.D. Cady, and J.J. Malloy, "The protected paste volume concept using new air-void measurement and distribution techniques," *J. Mater.*, **2**, 202 (1967).
59. K. Natesaiyer, K.C. Hover, and K.A. Snyder, "Protected-paste volume of air-entrained cement paste. Part I," *J. Mater. Civ. Eng.*, **4**, 166 (1992).
60. K. Natesaiyer, K.C. Hover, and K.A. Snyder, "Protected-paste volume of air-entrained cement paste. Part II," *J. Mater. Civ. Eng.*, **5**, 170 (1993).
61. S. Diamond, S. Mindess, and J. Lovell, "On the spacing between aggregate grains in concrete and the dimension of the aureole de transition"; in *Liaisons Pâtes de Ciment/Matériaux Associés.* International RILEM Colloquium (Toulouse), C42. 1982.
62. D.P. Bentz and K.A. Snyder, "Protected paste volume in concrete: Extension to internal curing using saturated lightweight fine aggregate," to be published in *Cem. Concr. Res.*
63. J. Marchand, R. Pleau, and R. Gagné, "Deterioration of concrete due to freezing and thawing"; p. 283 in *Materials Science of Concrete IV.* Edited by J. Skalny and S. Mindess. American Ceramic Society, Westerville, Ohio, 1995.
64. P. Hertz, "Über den gegenseitigen durchschnittlichen Abstand von Punkten, die mit bekannter mittlerer Dichte im Raume angeordnet sind," *Mathematische Annalen*, **67**, 387 (1909). See also Section VII of S. Chandrasekhar, "Stochastic problems in physics and astronomy," *Rev. Modern Phys.*, **15**, 1 (1943).
65. K. Natesaiyer, M. Simon, and K. Snyder, "Discussion of 'Mean spacing of air voids in hardened concrete' by E. Attiogbe," *ACI Mater. J.*, **91**, 123 (1994).
66. E.K. Attiogbe, "Volume fraction of protected paste and mean spacing of air voids," *ACI Mater. J.*, **94**, 588, 1997.
67. M. Abramowitz and I.A. Stegun, eds., *Handbook of Mathematical Functions.* Dover Publications, Inc., New York, 1972.
68. G. Arfken, *Mathematical Methods for Physicists.* Academic Press, New York, 1970.
69. K.A. Snyder, "Discussion of 'The use of the flow length concept to assess the efficiency of air entrainment with regards to frost durability: Part I — Description of the test method,'" *Cem. Concr. Aggregates*, **19**, 116, 1997.
70. K.A. Snyder, D.N. Winslow, D.P. Bentz, and E.J. Garboczi, "Effects of interfacial zone percolation in cement-aggregate composites"; p. 265 in *Advanced Cementitious Systems: Mechanisms and Properties.* Materials Research Society, 1992.

71. K.A. Snyder, D.N. Winslow, D.P. Bentz, and E.J. Garboczi, "Interfacial zone percolation in cement-aggregate composites"; p. 259 in *Interfaces in Cementitious Composites*. Edited by J.C. Maso. RILEM, 1992.
72. D.N. Winslow, M.D. Cohen, D.P. Bentz, K.A. Snyder, and E.J. Garboczi, "Percolation and pore structure in mortars and concrete," *Cem. Concr. Res.*, **24**, 25 (1994).
73. D.P. Bentz, J.T.G. Hwang, C. Hagwood, E.J. Garboczi, K.A. Snyder, N. Buenfeld, and K.L. Scrivener, "Interfacial zone percolation in concrete: Effects of interfacial zone thickness and aggregate shape"; p. 437 in *Microstructure of Cement-Based Systems: Bonding and Interfaces in Cementitious Materials*. Edited by S. Diamond, S. Mindess, F.P. Glasser, L.W. Roberts, J.P. Skalny, and L.D. Wakeley. Materials Research Society, Pittsburgh, 1995.
74. E.J. Garboczi and D.P. Bentz, "Analytical formulas for interfacial transition zone properties," *Adv. Cem. Based Mater.*, **6**, 99 (1997).
75. E.J. Garboczi and D.P. Bentz, "Multi-scale analytical/numerical theory of the diffusivity of concrete," *Adv. Cem. Based Mater.*, **8**, 77, 1998.
76. S.B. Lee and S. Torquato, "Porosity for the penetrable-concentric-shell model of two-phase disordered media: computer simulation results," *J. Chem. Phys.*, **89**, 3258 (1988).
77. J. Vieillard-Baron, "Phase transitions of the classical hard-ellipse system," *J. Chem. Phys.*, **56**, 4729 (1972).
78. A.L.R. Bug, S.A. Safran, G.S. Grest, and I. Webman, "Do interactions raise or lower a percolation threshold?" *Phys. Rev. Lett.*, **55**, 1896 (1985).
79. H. Reiss, H.L. Frisch, and J.L. Lebowitz, "Statistical mechanics of rigid spheres," *J. Chem. Phys.*, **31**, 369 (1959).
80. H. Reiss and R.V. Casberg, "Radial distribution function for hard spheres from scaled particle theory, and an improved equation of state," *J. Chem. Phys.*, **61**, 1107 (1974).
81. J.R. MacDonald, "On the mean separation of particles of finite size in one to three dimensions," *Molec. Phys.*, **44**, 1043, 1981.
82. S. Torquato and S.B. Lee, "Computer simulations of nearest-neighbor distribution functions and related quantities for hard-sphere systems," *Physica A*, **167**, 361 (1990).
83. S. Torquato, B. Lu, and J. Rubinstein, "Nearest-neighbor distribution functions in many-body systems," *Phys. Rev. A*, **41**, 2059 (1990).
83. P.A. Rikvold and G. Stell, "D-dimension interpenetrable-sphere models of random two-phase media: Microstructure and an application to chromatography," *J. Colloid Interface Sci.*, **108**, 158 (1985).
85. P.A. Rikvold and G. Stell, "Porosity and specific surface for interpenetrable-sphere models of two-phase random media," *J. Chem. Phys.*, **82**, 1014 (1985).
86. B. Lu and S. Torquato, "General formalism to characterize the microstructure of polydispersed random media," *Phys. Rev. A*, **43**, 2078 (1991).
87. W.F. Espenscheid, M. Kerker, and E. Matijevic, "Logarithmic distribution functions for colloidal particles," *J. Phys. Chem.*, **68**, 3093 (1964).
88. T.C. Powers, "Void spacing as a basis for producing air-entrained concrete," *Proc. ACI*, **50**, 741 (1954).
89. B. Warris, "The Influence of Air-Entrainment on the Frost Resistance of Concrete — Part B. Hypothesis and Freezing Experiments"; in *Swedish Cement and Concrete Research Institute Proceedings NR 36*. Stockholm, 1964.

90. M. Pigeon, R. Gagné, and C. Foy, "Critical air-void spacing factors for low water-cement ratio concretes with and without condensed silica fume," *Cem. Concr. Res.*, **17**, 896 (1987).
91. "Guide to the expression of uncertainty in measurement," Technical report, International Organization for Standardization (ISO), Genève, Switzerland, 1993.
92. B.N. Taylor and C.E. Kuyatt, "Guidelines for evaluating and expressing the uncertainty of NIST measurement results," Technical report, National Institute of Standards and Technology, Gaithersburg, Maryland, 1993.
93. J. Mandel, *The Statistical Analysis of Experimental Data.* Interscience Publishers, New York, 1964.
94. E.B. Wilson, *An Introduction to Scientific Research.* McGraw-Hill, New York, 1952.
95. J.R. Taylor, *An Introduction to Error Analysis,* 2nd ed. University Science Books, 1997.
96. R.H. Dieck, *Measurement Uncertainty: Methods and Applications,* 2nd ed. Instrument Society of America, 1997.
97. P.L. Meyer, *Introductory Probability and Statistical Applications.* 2nd ed. Addison-Wesley, Reading, 1970.
98. W. Feller, *An Introduction to Probability Theory and its Applications,* vol. I. John Wiley & Sons, New York, 1950.
99. M.J. Lighthill, *Introduction To Fourier Analysis and Generalised Functions.* Cambridge University Press, Cambridge, 1958.